

FOCUSING OPTICS FOR X-RAY APPLICATIONS

BY

KRISTINA YOUNG

DEPARTMENT OF MECHANICAL, MATERIALS, AND AEROSPACE
ENGINEERING

Submitted in partial fulfillment of the
requirements for the degree of
Masters of Science in Materials Science and Engineering
in the Graduate College of the
Illinois Institute of Technology

Approved _____
Adviser

Chicago, Illinois
July 2005

ACKNOWLEDGEMENT

First and foremost I'd like to thank Dr. Sheldon Mostovoy for encouraging me to continue pursuing a higher degree in materials science. His caring and kindness pushed me to work harder if his tough questions failed to do so. I thank my advisor Dr. Philip Nash for his gentle guidance and encouragement during my research. I'd also like to thank Dr. Ali Khounsary at Argonne National Laboratory's Advanced Photon Source. His commitment to mentoring students to become successful scientists in the field allowed me the opportunity to work in a challenging environment amongst world class minds. I offer much thanks to Gabriel Lucas and Buehler Ltd. for their services with regard to polishing the aluminum CRL lens samples, for the samples of replicating media they supplied, as well as for their advice when metallographic questions arose. Lastly, I'd like to thank all the faculty and staff at both IIT and Argonne for their time support which helped me to learn and do what was necessary to perform my work.

TABLE OF CONTENTS

	Page
ACKNOWLEDGEMENT	iii
LIST OF TABLES	vi
LIST OF FIGURES	vii
LIST OF SYMBOLS	viii
ABSTRACT	ix
CHAPTER	
1. DEVELOPMENT OF X-RAY OPTICS	1
1.1 Grazing Incidence Mirrors	1
1.2 Fresnel Zone Plates	4
1.3 Compound Refractive Lenses	5
2. X-RAYS AND THEIR INTERACTIONS WITH MATTER	8
2.1 Discovery of X-Rays	8
2.2 Synchrotron Radiation	8
2.3 Reflection and Refraction of X-Rays	11
2.4 Scattering of X-Rays	13
2.5 Absorption of X-Rays	13
3. GRAZING INCIDENCE FOCUSING MIRROR SIMULATION	15
3.1 Design of Focusing Mirror Configuration	16
3.2 Mirror Fabrication	16
3.3 Beamline 34ID Layout	17
3.4 Tolerancing Mirror Alignments	18
3.5 SHADOW Roughness Modeling	23
4. ALUMINUM COMPOUND REFRACTIVE X-RAY LENS	28
4.1 Design	28
4.2 Fabrication	28
4.3 Testing	30
5. LITHIUM COMPOUND REFRACTIVE X-RAY LENS	36
5.1 Material Properties of Lithium Metal	38
5.2 Design of a Lithium CRL	40
5.3 Fabrication of Lenslets	47
5.4 Characterization of Lenslet Profiles	49
5.5 Testing of a Lithium Compound Refractive Lens	52
5.6 Future Work	56

APPENDIX

A. CAD DRAWINGS OF LITHIUM LENS DESIGNS.....	58
B. SAFE HANDLING OF LITHIUM.....	63
BIBLIOGRAPHY	70

LIST OF TABLES

Table	Page
3.1 Design Parameters of Focusing Mirrors	16
3.2 SHADOW and Hand Calculated Image Sizes.	19
3.3 Simulated vs. Experimental Results.....	26
5.1 General Material Properties of Lithium Metal.....	38
5.2 Statistics of Replicated Sample Measurements.....	52

LIST OF FIGURES

Figure	Page
1.1 Illustration of Kirkpatrick-Baez Mirror Configuration.....	2
1.2 Cartoon of a Design Ellipse for a Given Optical Layout.....	3
1.3 SEM Image of a Fresnel Zone Plate.....	4
1.4 Schematic of a CRL Array Focusing an Incident Ray.....	6
2.1 The Electromagnetic Spectrum.....	9
2.2 A Simple Schematic of a Synchrotron Storage Ring.....	10
2.3 Spectral Brightness of Various Radiation Sources.....	11
2.4 Schematic Representing Snell’s Law.....	12
3.1 Configuration of KB-Mirrors.....	17
3.2 Illustration of Experimental Beamline Layout.....	17
3.3 Mirror Misalignment Axes.....	18
3.4 Spot Size vs. Roll Misalignment of Vertically Focusing Mirror.....	19
3.5 Spot Size vs. Roll Misalignment of Vertically Focusing Mirror.....	20
3.6 Spot Size vs. Roll Misalignment of Horizontally Focusing Mirror.....	20
3.7 Spot Size vs. Roll Misalignment of Vertically Focusing Mirror.....	20
3.8 Ray-tracing Results for Various Types of Mirror Misalignment.....	22
3.9 SHADOW Simulated Focal Spot with Ideal KB Mirrors.....	24
3.10 Vertical Spot Size vs. Mirror Position.....	25
3.11 Horizontal Spot Size vs. Mirror Position.....	25
3.12 Smallest Simulated Focal Spot.....	26
3.13 Smallest Vertical Focal Spot Size Measured at APS Beamline 34ID.....	27
3.14 Smallest Horizontal Focal Spot Size Measured at APS Beamline 34ID.....	27
4.1 Schematics of Extrusion Apparatus.....	29

Figure		Page
4.2	Fabrication of the Aluminum CRL Array.....	30
4.3	Photo of Manufactured CRL.....	30
4.4	Schematic of Aluminum CRL Beamline Layout.....	31
4.5	Calculated and Experimental Transmission Profiles.....	32
4.6	Measured and Normalized Intensity Profiles of the X-ray Beam at the Image Distance.....	32
4.7	Vertical Beam Size (FWHM) of the X-ray Beam Downstream from the Lens.....	33
4.8	Comparison of First (left) and Second (right) Generation Al CRL Profiles.....	35
5.1	True Stress vs. True Strain of Lithium.....	38
5.2	Refractive Index Decrement over Absorption vs. Energy.....	39
5.3	Reactivity of Lithium with Air.....	39
5.4	Schematic of the Cross-section of Lithium Reaction Products.....	40
5.5	Photo of Pressing Fixture Employed to Press Lithium Lenslets.....	41
5.6	Rockwell Hardness Indenter with Ball Tip.....	43
5.7	Unpolished (left) and Electropolished (right) 440c Stainless Steel Parabolic Indenters.....	43
5.8	Unpolished (left) and Electropolished (right) 316 Stainless Steel Parabolic Indenters.....	44
5.9	Lithium Lenslet Cartridge Unit.....	46
5.10	Photo of the Lens Array Assembly.....	46
5.11	Design Schematic of Lithium Lens Housing Unit.....	46
5.12	Schematic Diagram of a White Light Interferometer.....	50
5.13	Radius of Curvature vs. Roughness Measurements via White Light Interferometer.....	51
5.14	Schematic Layout of Beamline 7ID.....	53
5.15	Picture of Lithium Compound Refractive Lens in the Beamline.....	53
5.16	Plot of Focal Spot Size (FWHM) vs. Focal Length.....	54

Figure	Page
5.17 Intensity Profile of Smallest Focal Spot.....	54
5.18 3D Intensity Profiles of Focused and Unfocused Beam at the Focal Spot.	55
5.19 Transmission Profile of the Lithium Lens.....	56
5.20 Theoretical vs. Experimental Cumulative Thickness of Lithium Lenslets.	56

LIST OF SYMBOLS

Symbol	Definition
A	Atomic weight
a	Major axis of design ellipse
A_{eff}	Effective aperture
b	Minor axis of design ellipse
f	Focal Length
$f(0)$	Atomic scattering factor
f_1	Real portion of atomic scattering factor
f_2	Imaginary portion of atomic scattering factor
G	Gain
h	Planck constant
I	Final intensity of radiation wavefront
I_o	Initial Intensity of radiation wavefront
N	Refractive index of a material
N_A	Avagadro's number
N_z	Diffraction order
n	Index of refraction
n_a	Index of refraction of media A
n_b	Index of refraction of media B
n_i	Number of atoms per unit volume
n_z	Zone Number
R	Radius of curvature of lens profile
r_e	Classical electron radius
r_n	Radius of zone number n

Symbol	Definition
S	Source distance
S'	Image distance
T	Percent transmission
v	Speed of light
β	Absorption index of a material
δ	Index of refraction decrement
θ	Angle of incidence
θ_a	Incident angle
θ_b	Angle of refraction
θ_c	Critical angle
θ_r	Angle of reflection
λ	Wavelength of radiation
μ	Total photoeffect attenuation coefficient
μ_A	Coefficient of absorption
ρ	Density of a material
σ	Coefficient of absorption due to scattering
σ_s	<i>rms</i> source size
τ	Coefficient of true absorption

ABSTRACT

There is a growing demand for focused or collimated x-ray beams in a variety of engineering and scientific applications. Such beams allow the examination of samples and specimens with high spatial resolution and/or high system throughput. Micro- and nano-sized x-ray beams can be instrumental in understanding many biological and physical systems.

There are a number of techniques to focus or collimate x-ray beams. These rely on the use of mirrors, zone plates, x-ray lenses, capillary lenses, and crystals to name a few. While each technique has its own advantages and disadvantages, each optic has its own place in x-ray instrumentation.

Analyses of the performance of grazing incidence mirrors, and the fabrication and analysis of compound refractive lenses composed of aluminum and lithium are discussed. The performance of two orthogonally placed grazing incidence Kirkpatrick-Baez mirrors each focusing in one direction has been analyzed via SHADOW ray-tracing with respect to both the tolerance and alignment of such mirrors as well as accounting for the surface roughness of the mirrors in determining the location of the smallest focal spot. The performance of an extruded aluminum compound refractive lens having lenslet radii and wall thicknesses of 0.5 mm and 150 μm has been analyzed. This wall thickness is the smallest hot micro-multi-port extruded structure to date. Lithium compound refractive lenslets have been fabricated in a high precision die press with both spherical and parabolic profiles with radii of 0.790 mm and 0.1 mm (radius of parabolic tip) respectively. The quality of the lenslets is analyzed via white light interferometer with respect to both figure and finish. The performance of a parabolic lithium compound refractive lens with a focal length of 1.7 m was analyzed at 10keV.

CHAPTER 1

DEVELOPMENT OF X-RAY OPTICS

Since the discovery of x-rays, x-ray analysis has been employed as a tool to examine and investigate phenomena in a broad range of fields from geology, to biology, materials science, medicine, and computer science. There are a number of references that highlight the development of x-rays in scientific research [Mich96]. There is a demand however, for focused/collimated x-ray beams. Such beams allow the examination of samples and specimens with high spatial resolution and/or high system throughput. Micro- and nano-beams are essential for understanding many biological [Sim99] and physical [Math99]¹ systems, as they can penetrate opaque samples non-destructively.

There are a number of methods to focus x-ray beams including but not limited to grazing incidence mirrors [Kirk48], Fresnel zone plates [Yang93], and compound refractive lenses (CRL) [Snig96]. Each method has its own advantages and disadvantages depending upon the application, and is introduced in this chapter. Each method also takes advantage of how x-rays interact with matter. These phenomena are outlined in Chapter 2. Chapter 3 outlines the design, fabrication, and ray-tracing simulation of grazing incidence mirrors. Chapters 4 and 5 outline the development and analysis of novel techniques being used to fabricate CRLs from aluminum and lithium.

1.1 Grazing Incidence Mirrors

Total external reflection mirrors were one of the first means of focusing x-rays after Compton had observed the reflection of x-rays at glancing angles [Compt23]. Reflectivity is the ratio of the intensity of the total radiation reflected from a surface to the total incident radiation on that surface [Hec90].

¹ Corresponding to references in the Bibliography

Mirrors used to focus x-rays can be figured or bent to a specific shape to achieve the desired focusing. The advantages of mirrors include high beam throughput and no chromatic aberration compared to other focusing optics such as zone plates. Chromatic aberrations occur when radiation of different wavelengths are focused to different points along the optical axis. Point-to-point (two-dimensional) focusing can be performed with an ellipsoidal mirror profile however the first mirrors to focus x-rays were suggested and employed by Kirkpatrick and Baez [Kirk48]. They used a two mirror system in which one mirror was responsible for focusing in a single direction. The two mirrors would be placed orthogonally with respect to each other and would be designed such that they both focus to the same point in space. Figure 1.1 below illustrates the Kirkpatrick-Baez mirror configuration.

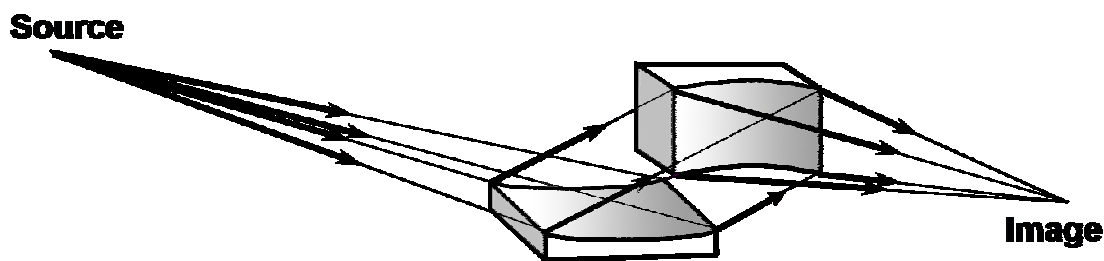


Figure 1.1. Illustration of Kirkpatrick-Baez Mirror Configuration.

This configuration allows mirrors to be machined or bent with an elliptical profile that is symmetrical about one axis (cylindrical) making the mirrors easier to fabricate than their ellipsoidal counterparts.

The profiles of elliptical mirrors are based on ellipses whose foci correspond to the source and image distances of the optical system as shown in Figure 1.2. Determining the ellipse profile is performed by using the equation of an ellipse (See Eqn. 1.1) with the desired source distance S , image distance S' and incident angle θ . The semi-major and semi-minor axes are determined using Equations 1.2 and 1.3.

$$\frac{x^2}{a^2} + \frac{y^2}{b^2} = 1 \quad (1.1)$$

$$a = \frac{S + S'}{2} \quad (1.2)$$

$$b = \sqrt{SS'} \sin \theta \quad (1.3)$$

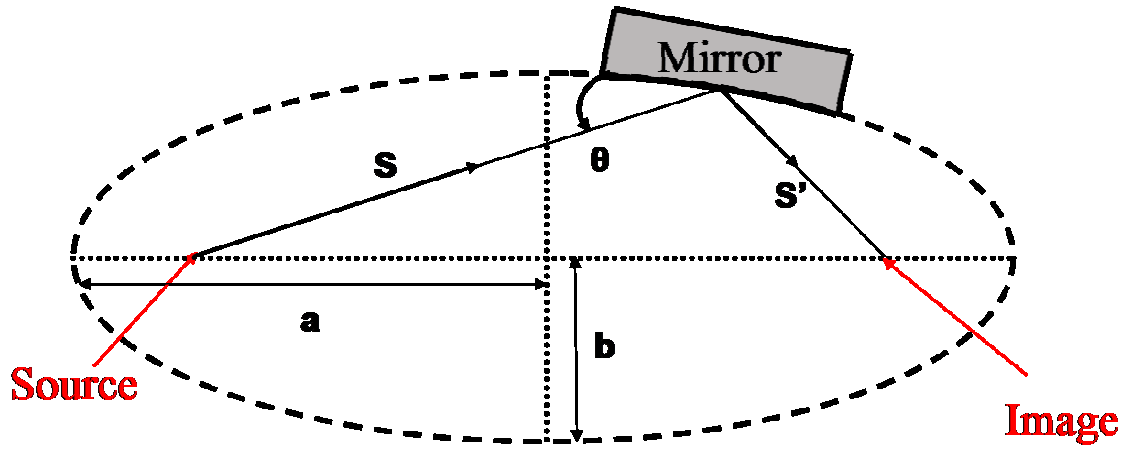


Figure 1.2. Cartoon of a Design Ellipse for a Given Optical Layout.

The performance of grazing incidence mirrors is strongly dependent on the slope errors present on their reflecting surfaces. Slope errors are height errors or bumps that change the incident angle of the incoming x-rays. The larger the slope, the further the x-ray beam will be reflected off its intended path. Slope errors are classified into two categories; figure and finish. Figure errors have low order spatial frequencies and detract from the overall geometry of the mirror such as its radius of curvature. They seriously blur the full-width at half maximum (FWHM) spot size of a focused beam. Slight figure errors on the order of 1 μ rad rms slope error can bring about focal spot sizes 10 times greater than the ideal. Finish errors have high order spatial frequencies and are the roughness of the mirror surface. Finish errors reduce the throughput and contrast of the focused beam. Information about the figure and finish of mirrors is presented in power spectral density plots and display the effects of figure and finish errors on the performance. Interested readers can refer to [Church95] for a detailed description of how power spectral density plots are created and interpreted.

Methods of improving the surface figure and finish of focusing mirrors have rested in their manufacture. Elastically bending flat substrates [How75] was initially the method of

choice for shaping mirrors because a flat substrate can be polished far better than an aspherical shape. However, it is difficult to accurately achieve the desired shape via bending and the mirror apparatus can be relatively large preventing the possibility of small focal lengths. New methods such as differential deposition [Ice00], plasma chemical vaporization [Yam03], and elastic emission machining [Yam03] are being employed to improve the surface characteristics of the mirrors with great success.

1.2 Fresnel Zone Plates

Fresnel zone plates (FZPs) have recently been employed in the x-ray region for focusing monochromatic beams and are analogous to Fresnel lenses used in the visible light region. A Fresnel zone plate typically consists of a plate with circular concentric ribs (See Fig. 1.3 [Fzp05]) and can be thought of as a circular diffraction grating. A diffraction grating consists of an array of parallel peaks and valleys that cause an incident beam to be diffracted. In certain directions, diffracted beams superimpose and in others they cancel. The diffraction angle is dependent on the wavelength of the radiation and the spacing between the peaks and valleys. Each peak or valley on a zone plate is called a zone and its radius from the center is determined by Equation 1.4 below. The peaks and valleys are spaced on a zone plate such that x-rays will cross the optical axis at the same point [Mich96].

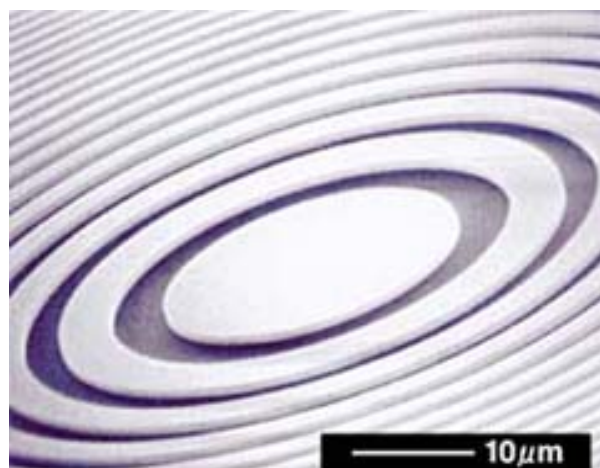


Figure 1.3. SEM Image of a Fresnel Zone Plate.

The radius of the zone is dependent upon N_z , the diffractive order used for imaging, n the zone number, λ the wavelength of radiation, and f the focal length.

$$r_n^2 = N_z n_z \lambda f + \frac{N_z^2 n_z^2 \lambda^2}{4} \quad (1.4)$$

Initially, zone plates used concentric ribs as opaque regions to block the destructive interference amplitudes increasing the intensity of the focal spot. The efficiency of Fresnel zone plates of this type are very poor amounting to only 10% of the input radiation traversing the zone plate. Improvements on this initial design have been to induce a phase shift of π on the wavefront of the x-ray beam in the optical path length from the source to the focal length in each zone as opposed to blocking the destructive amplitude. This increases the efficiency of the optic to 40%.

The spatial resolution of a Fresnel zone plate is limited by the width of the outermost zone. The width of these zones is restricted by the technology available to fabricate them and is on the order of 30 nm. Nevertheless, zone plates are the optic of choice for very low energies and can focus x-ray beams down to the micron and nanometer scale.

1.3 Compound Refractive Lenses

Compound refractive lenses (CRLs) are arrays of lenses designed to focus x-rays. CRLs are desirable due to their simple designs and ease in implementation and alignment. A CRL generally consists of an array of double concave lenses such that each lens contributes only a small portion of the total bending (focusing) of the x-ray beam (See Fig. 1.4). Introducing an array of lenses reduces the focal length to a manageable distance for beamline applications. Given an x-ray lens array with N lenses each having a radius of curvature R , and an index of refraction decrement δ the focal length is given by Equation 1.5. The real index of refraction decrement accounts for the amount a material refracts (bends) incident radiation. Typically, values of δ are on the order of 10^{-5} to 10^{-6} , and, if a single lens were to be used to focus an x-ray, its focal length would be hundreds of meters long.

$$F = \frac{R}{2N\delta} \quad (1.5)$$

Absorption is a limiting factor affecting x-ray lenses as it reduces the transmission of a lens. Therefore, materials high refraction and low absorption are desirable as CRLs. Materials with this attribute include lithium, beryllium, carbon, aluminum and each may be preferred over others for a given energy range or method of fabrication.

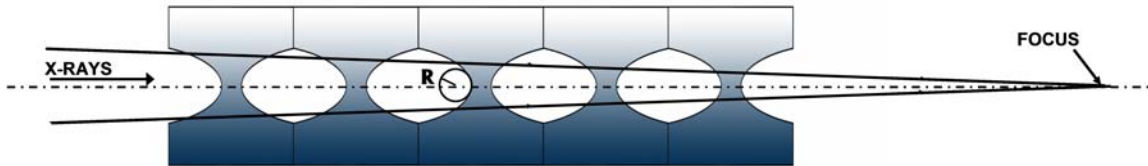


Figure 1.4. Schematic of a CRL Array Focusing an Incident Ray.

X-ray lenses were long thought to be an impractical means of focusing x-rays. Yang [Yang93] reexamined the feasibility of x-ray lenses and determined that, in the lower eV range (30-1000), only low-Z materials, such as hydrogen, lithium, and beryllium, would provide beneficial focusing and noted that fabrication using such materials was impractical. The first CRL was fabricated by drilling holes into aluminum blocks creating cylindrical lenses capable of one-dimensional focusing [Snig96]. Two-dimensional focusing CRLs were made by cross drilling into the material [Snig98]. Parabolic and paraboloidal [Leng99] CRLs have also been developed to address spherical aberrations and have proven to be successful. Spherical aberrations occur because spherical lenses and mirrors do not focus rays to a point but rather along a line. This is because off-axis rays are focused to the optical axis at a shorter distance than those that are on the axis. Efforts have since concentrated on fabrication techniques that reduce the wall thickness and radius of curvature and improve the surface quality of the lenses. One such technique to note is the multi-prism or saw-tooth lens [Ced02], which mimics a parabolic profile by using teeth imprinted or etched onto two identical planar strips that act as jaws to vary the focal length of the lens. The opening and closing of the jaws induce the adjustment in the focal length. Other fabrication techniques include stamping

[Ced02] and lithography [Schr02] [Manc02]. Fabrication and analysis of aluminum and lithium compound refractive lenses is given in Chapters 4 and 5.

CHAPTER 2

X-RAYS AND THEIR INTERACTIONS WITH MATTER

X-ray physics has grown significantly since its inception in 1895. Scientists immediately recognized the potential of x-rays and delved into developing experiments that would shed light on how they interact with matter compared to other forms of radiation. Research into how x-rays are reflected, refracted, absorbed, diffracted, and scattered was conducted and yielded considerable insight as to how x-rays could further be used in a variety of applications that are now employed today.

2.1 Discovery of X-Rays

X-rays were discovered by W. C. Roentgen in 1895 while systematically researching any radiation that could penetrate matter where visible light could not [Compt54]. Roentgen termed the radiation “x-rays” highlighting their unknown behavior. His experiments yielded the following observations [Bro66] and earned him the Nobel Prize in 1901:

- Substances fluoresce under irradiation.
- Photographic plates and films are sensitive to x-rays.
- X-rays are not deflected by magnetic fields.
- X-rays travel in straight lines.
- X-rays are generated whenever cathode rays strike a solid body. Heavier elements are more effective producers of x-rays.

2.2 Synchrotron Radiation

Synchrotron radiation is a form of electromagnetic radiation that is emitted when charged particles travel at relativistic velocities along curved paths [Win94]. It was first observed in 1947 at the General Electric Research Laboratory and was employed in research in the 1960’s. Synchrotron radiation exists in wavelengths in the electromagnetic spectrum as shown below in Figure 2.1 [Win94].

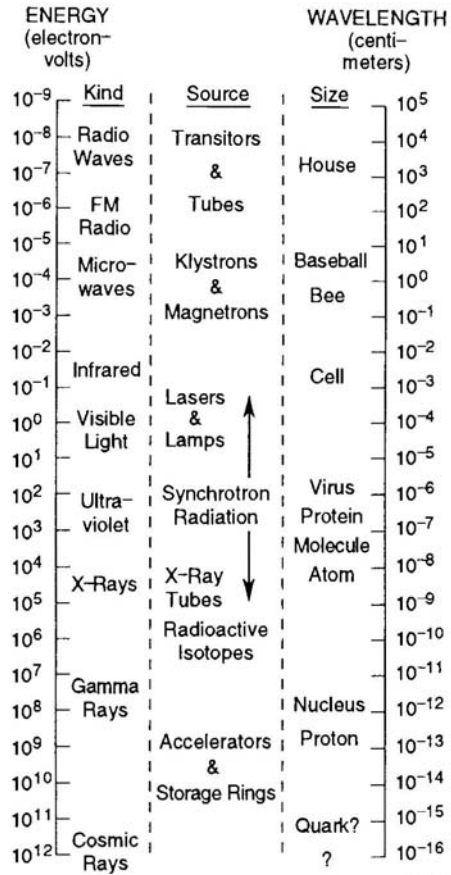


Figure 2.1. The Electromagnetic Spectrum.

The first x-ray source solely dedicated to generating and studying synchrotron radiation was brought online in 1980 and is the Synchrotron Radiation Source (SRS) in Daresbury Laboratory in the UK. It is still in operation and operates at 2 GeV electron energy. Since the SRS, second and third generation synchrotron sources have been constructed, the three largest being SPring8 in Japan operating at 8 GeV, the Advanced Photon Source (APS) in the US operating at 7 GeV, and European Synchrotron Radiation Facility (ESRF) in France operating at 6 GeV. The above facilities all rely on storage ring components to maintain a constant flow of electrons traveling near the speed of light for several hours (See Fig. 2.2) [Win94].

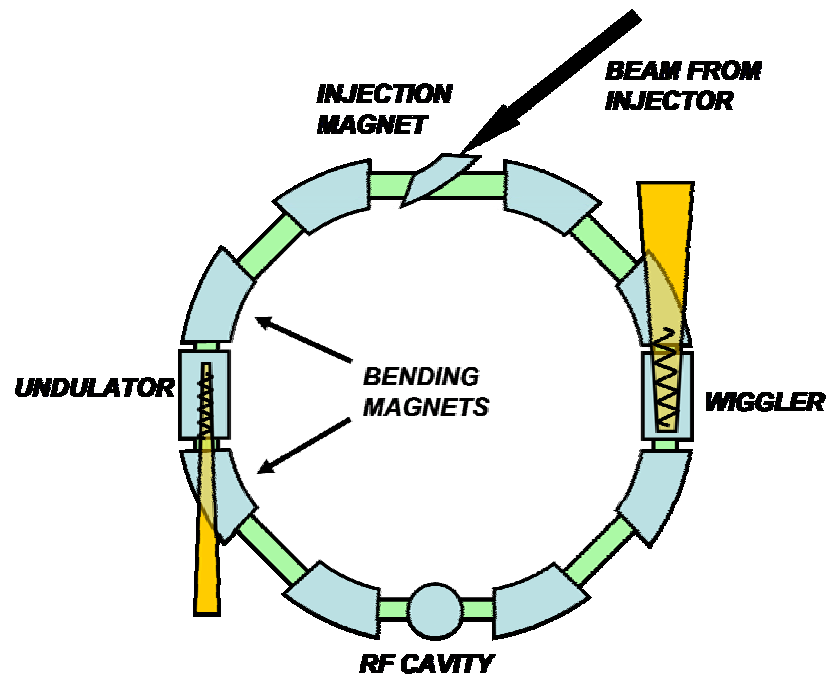


Figure 2.2. A Simple Schematic of a Synchrotron Storage Ring.

Bending magnets continuously change the direction of the path of the x-rays to accommodate a curved path around the storage ring. The arrangement of the magnets affects the characteristics of the circulating beam and is called the lattice. The energy of the electrons in the storage ring is maintained by radio frequency (*rf*) cavities that emit electromagnetic waves in radio frequencies to excite the electrons. Undulators and wigglers are a series of magnets with alternating poles intended to force electrons to move according to a periodic wave structure and emit more radiation. The periodic structure is designed such that there is no net bending allowing for these components to be placed in straight sections of a beamline or storage ring [Win94]. Figure 2.3 shows the relative brightness of various radiation sources [Win94].

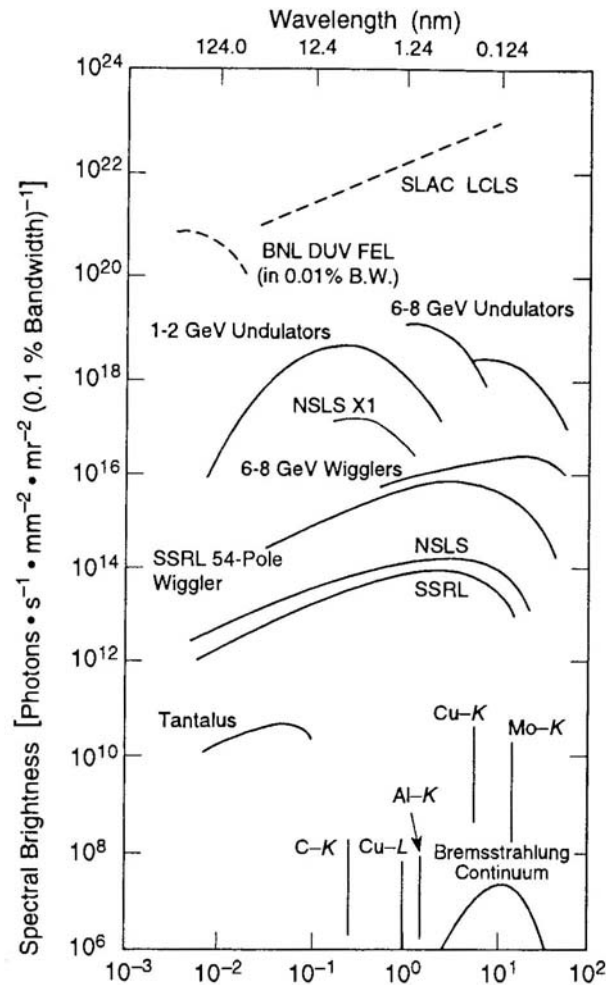


Figure 2.3. Spectral Brightness of Various Radiation Sources.

2.3 Reflection and Refraction of X-Rays

Roentgen had unsuccessfully attempted to observe both reflection and refraction of x-rays. Reflection refers to radiation encountering an interface of another media at a given angle and is redirected (reflected) away from the media at an equal and opposite angle. Refraction refers to the transmission of radiation from one media to another at a given angle. If the incident angle is not perpendicular to the media interface, the radiation will be slightly redirected (bent) off its original path by a given angle. The first observation of refraction was credited to Stenström in 1919 [Compt54] and reflection was observed later by Compton in 1923 [Compt23]. Stenström's results indicated that the index of refraction of all materials with respect to x-rays was slightly less than one. The index of refraction dictates the amount

by which an incident ray of light or x-ray is altered in direction when passing from one media to another (See Fig. 2.4). Snell's Law predicts the amount of reflection and or refraction that occurs and is given by Equation 2.1 [Born99].

$$\frac{\sin \theta_a}{\sin \theta_b} = \frac{n_b}{n_a} \quad (2.1)$$

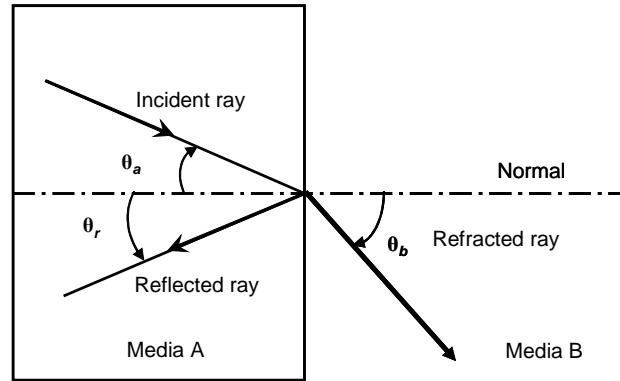


Figure 2.4 Schematic Representing Snell's Law.

The index of refraction of a material is given by Equation 2.2 below [Hen93],

$$n = 1 - \delta - i\beta = 1 - \frac{r_e}{2\pi} \lambda^2 \sum_{i=1}^N n_i f_i(0), \quad (2.2)$$

where δ represents the real index of refraction decrement and accounts for the amount a material refracts (bends) incident radiation upon encountering an interface, β represents the absorption index, r_e is the classical electron radius, λ is the wavelength of the incident radiation, and n_i is the number of atoms per unit volume. Quantities δ and β are related to the atomic scattering factor in the forward direction $f(0)$, Equation 2.3 below. The atomic scattering factor gives the efficiency of an atom scattered in a particular direction by comparing the amplitude of the wave of the atom with the wave of a free electron.

$$f(0) = f_1 + if_2 \quad (2.3)$$

The real portion of the atomic scattering factor f_1 is related to δ with Equation 2.4, but can be approximated by the atomic number of the material Z at energies higher than 1 keV [Hen82].

$$\delta = f_1 \frac{r_e \lambda^2}{2\pi} \frac{N_A}{A} \rho \quad (2.4)$$

A is the atomic weight of the material, N_A is Avagadro's number and ρ is the density of the material. The imaginary portion, f_2 is related to the total photoeffect attenuation coefficient μ with Equation 2.5 [Hen93].

$$\mu(h\nu) = \frac{4\pi\beta}{\lambda} = 2n_i r_e \lambda f_2 \quad (2.5)$$

Implications of the refractive index of materials being less than one in the x-ray region is the that x-rays may only be reflected at grazing angles via total external reflection. This is shown with calculation of the critical angle θ_c which is given by Equation 2.6. The refractive index decrement δ dictates the critical angle and is typically in the range of 10^{-4} to 10^{-6} making critical angles in the range of 1 to 14 mrad (0.08 to 0.81 degrees).

$$\theta_c = \sqrt{2\delta} \quad (2.6)$$

2.4 Scattering of X-Rays

Scattered x-rays are those that travel in directions other than the direction of incidence. Scattering and absorption are additive effects and can be related to the absorption coefficient of an alloy by Equation 2.7 below [Compt54],

$$\mu_A = \tau + \sigma \quad (2.7)$$

where μ_A is the coefficient of absorption, τ is the coefficient of true absorption and σ is the coefficient of absorption due to scattering.

2.5 Absorption of X-Rays

It was observed during Roentgen's earliest experiments that an x-ray's ability to traverse a material was dependent upon the atomic number of the element or the average atomic number of the material's constituent elements. Materials with higher atomic numbers tend to absorb more x-rays than those with lower atomic numbers. This realized by measuring the intensity of the x-ray beam before and after passing through a material of a given

thickness. The resulting relationship given in Equation 2.8 gave notion to the concept of the “absorption coefficient” where I is the intensity of the beam after traversing a material of thickness x , I_o is the initial intensity of the beam and μ is the absorption coefficient of the given material. The absorption coefficient represents the fractional decrease in intensity produced as the beam traverses a unit distance.

$$I = I_o e^{-\mu x} \quad (2.8)$$

The absorption coefficient can be described two ways; as a linear absorption coefficient and as a mass absorption coefficient. The linear absorption coefficient is of more importance in x-ray optics because it quantifies the amount of energy absorbed per unit length. The mass absorption coefficient quantifies how much energy is absorbed per unit mass of material.

CHAPTER 3

GRAZING INCIDENCE FOCUSING MIRROR SIMULATION

Advances in the development of grazing angle focusing optics have predominantly been in their fabrication. Machining and polishing techniques as mentioned in Chapter 1 have improved the quality of reflecting surfaces of the mirrors on the order of $0.6 \mu\text{rad}$ root mean square (*rms*) or better have been achieved [Ice04]. The design goal for focusing mirror optics is to achieve focal spot sizes near the diffraction limit. The diffraction limit restricts the imaging quality of the optic and has a greater affect (blurring) as the physical dimensions of the optic approach the wavelength of the incident radiation [Hec90]. Before the diffraction limit can be reached, slope errors on mirror optics would have to be on the order of $0.2 \mu\text{rad}$ root mean square (*rms*) or better [Ice04].

Modeling can serve as a useful aid in the design and use of mirror optics by accounting for slope errors and determining the optimal positioning of the mirrors to find the smallest focal spot. This chapter discusses the simulation of a nano-focusing Kirkpatrick-Baez (KB) mirror configuration designed and commissioned for use at the Advanced Photon Source at Argonne National Laboratory. Two types of simulations were performed. The first investigated the alignment requirements of a perfect KB system with respect to how much the two mirrors can deviate from being perfectly orthogonal to each other. The second type of simulations incorporated metrology data (slope errors) measured from the actual mirrors used on the beamline to determine whether any adjustments in the mirrors' positions along the x-ray beam path can minimize the blurring caused by slope errors. The simulations were performed using SHADOW ray-tracing software. SHADOW is a part of an x-ray software package called XOP [Rio98] developed for synchrotron radiation scientists and users.

3.1 Design of Focusing Mirror Configuration

Design of the KB mirror configuration was based upon the layout of beamline 34ID at the APS as well as by the needs of its users. The first mirror in the configuration focuses vertically and has a focal length of 60 mm. The second mirror focuses horizontally and has a focal length of 30 mm. The mirrors are designed to demagnify a source 60 m away by 1000 times in the vertical and 2000 times in the horizontal directions. For example, if an unobstructed source generates a beam size of 3 mm (h) x 1 μm (v) 60 m away it would be focused to 1.5 μm (h) x 1 nm (v) using perfect mirrors described above. Table 3.1 below relays the mirror parameters reflecting this design.

Table 3.1. Design Parameters of Focusing Mirrors.

Mirror	Vertically Focusing	Horizontally Focusing
Substrate Material	Float zone single crystal Si	Float zone single crystal Si
Length (mm)	40	20
Width (mm)	20	20
Focal length (mm)	60	30
Incident Angle (mrad)	3	3
Acceptance (μm)	120	60
Major-axis of ellipse a (m)	30.03	30.03
Minor-axis of ellipse b (mm)	5.692	4.062

3.2 Mirror Fabrication

Once the necessary design parameters of the mirrors were established the mirrors were fabricated. Fabrication of the nano-focusing vertically focusing mirror involved a proprietary computer controlled differential polishing processes developed by Tinsley Laboratories for production of ultra-smooth aspheric surfaces. This process was deemed feasible to produce mirrors with *rms* slope errors less than 0.2 micro radians [Tin02]. The horizontally focusing mirror was produced via differential deposition of the mirror surface to achieve the desired mirror profile. The mirrors are shown below (See Fig.3.1).

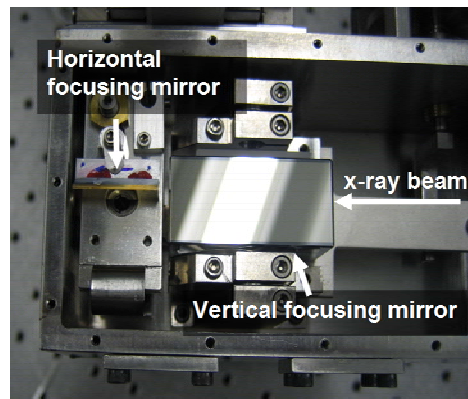


Figure 3.1. Configuration of KB-Mirrors.

3.3 Beamline 34ID Layout

The fabricated mirrors were then installed and tested on beamline 34ID. The beamline consisted of the following components; an undulator source, an L5 slit, an aperture, the mirrors, and the detector. Figure 3.2 shows an illustration of the experimental beamline layout. The L5 slit is used to reduce the incoming horizontal beam size from $563\ \mu\text{m}$ to $100\ \mu\text{m}$ because the mirrors will only accept $60\ \mu\text{m}$ of the beam's width and the unused portion of the beam may interfere with the detector measurements downstream and needs to be blocked. The aperture is placed just before the mirrors eliminate any other portion of the beam that may not hit both mirrors and interfere with the focused beam measurements. The aperture can also be adjusted to illuminate a given areas of the mirror surfaces.

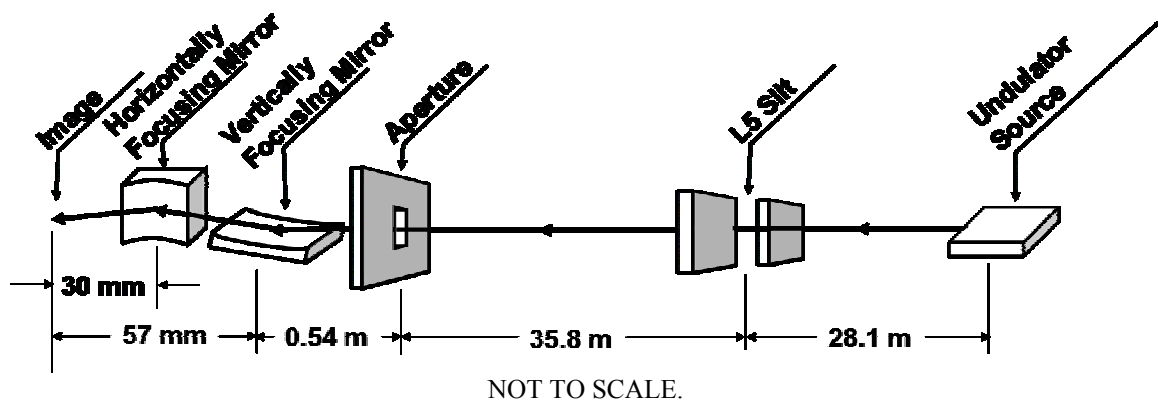


Figure 3.2 Illustration of Experimental Beamline Layout.

3.4 Tolerancing Mirror Alignments

KB mirror configurations require that the mirrors be as orthogonal to each other as possible. Any deviation from orthogonal alignment causes the mirrors to decouple and broaden the focused image because both mirrors no longer focus to the same point. Misalignment of the mirrors is possible in three directions roll, pitch and yaw as shown in Figure 3.3. Roll misalignment is synonymous with the orthogonal positioning of the mirrors and is not well understood. Simulations allow the opportunity to observe the effects and determine the limit of roll misalignment tolerated by a KB-mirror configuration.

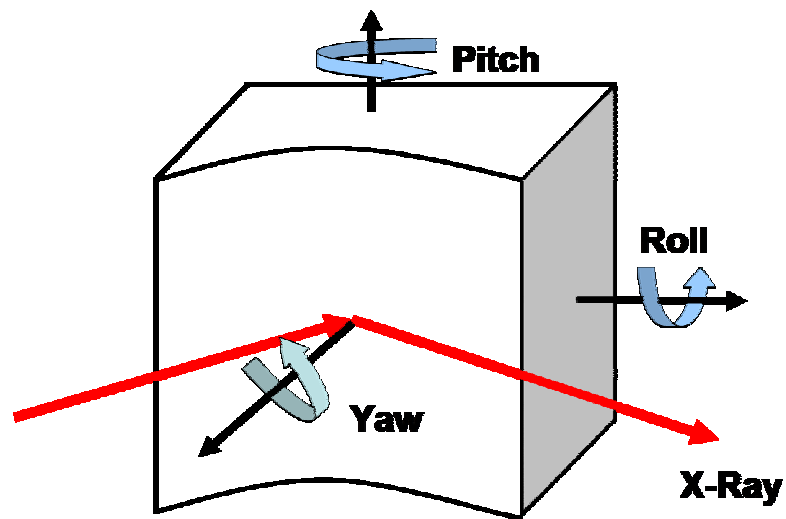


Figure 3.3. Mirror Misalignment Axes.

Modeling the mirror configuration begins with simulations for the case where the mirrors are perfectly orthogonal. This insures that all simulation parameters have been accounted for correctly and the resulting image agrees with expectations.

The source geometry employed was a 50 μm square with divergence to insure that the entire source is reflected by both mirrors. The results of a perfectly aligned run are in good agreement with calculations as shown in Table 3.2.

Table 3.2. SHADOW and Hand Calculated Image Sizes.

	Image Footprint [FWHM] Size		
	Hand Calculation	SHADOW Result	% Difference
Horizontal [nm]	25	22	12
Vertical [nm]	50	45	10

Next, simulations incorporating mirror misalignments are performed. Each mirror is misaligned with a roll rotation while the other remains at its ideal alignment. This is done to systematically identify the effects of misalignment of each mirror on the focal spot.

Implementing roll rotation of the first mirror yielded the results in Figures 3.4 and 3.5. The top figure includes gross misalignments of up to 2 degrees (35 mrad), while the bottom figure shows misalignments of up to 1 mrad. Likewise for the horizontally focusing mirror, Figures 3.6 and 3.7 show the effects of roll misalignment on the spot size.

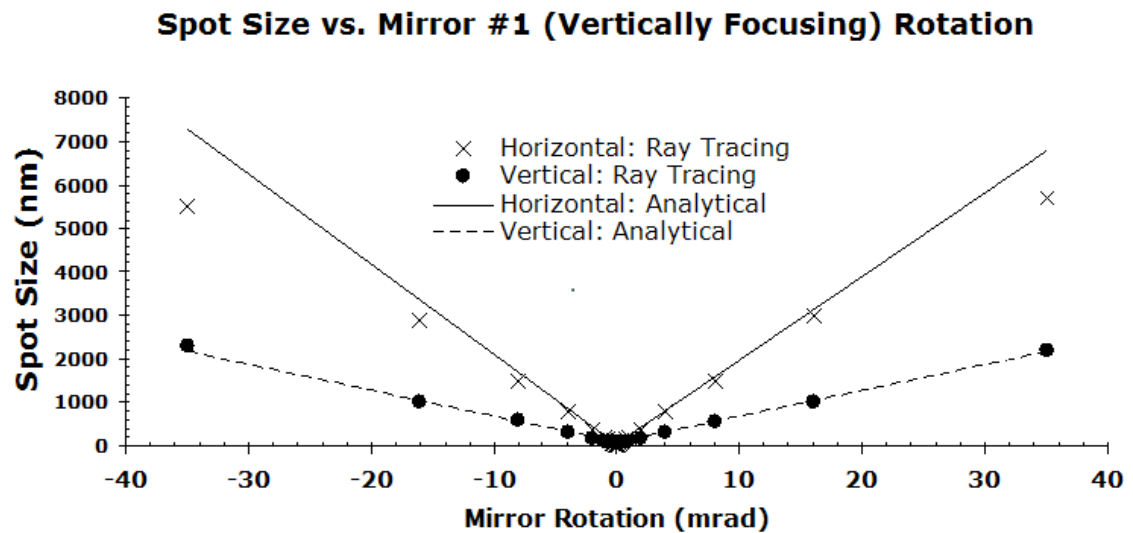


Figure 3.4. Spot Size vs. Roll Misalignment of Vertically Focusing Mirror.

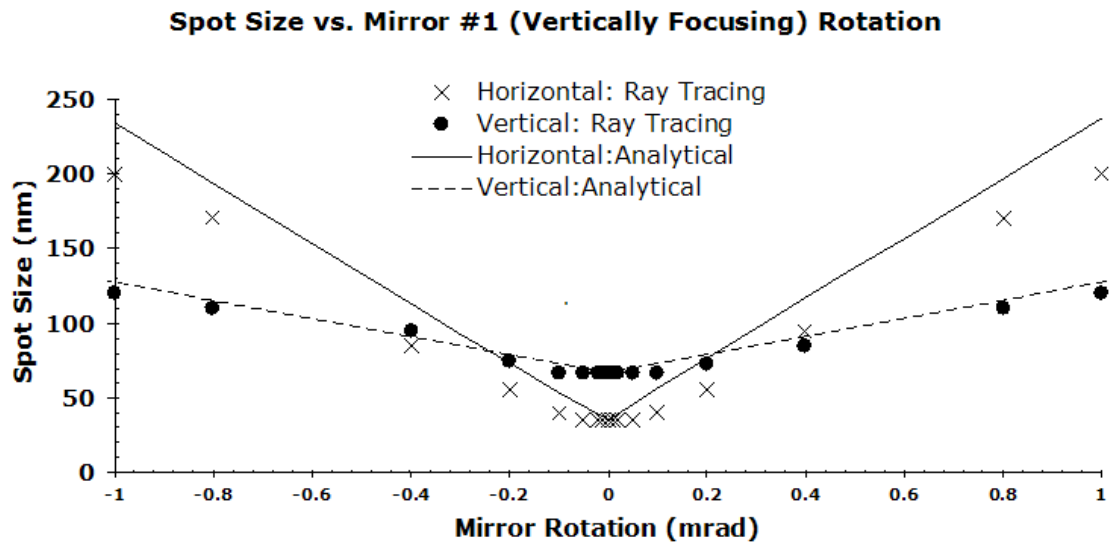


Figure 3.5. Spot Size vs. Roll Misalignment of Vertically Focusing Mirror.

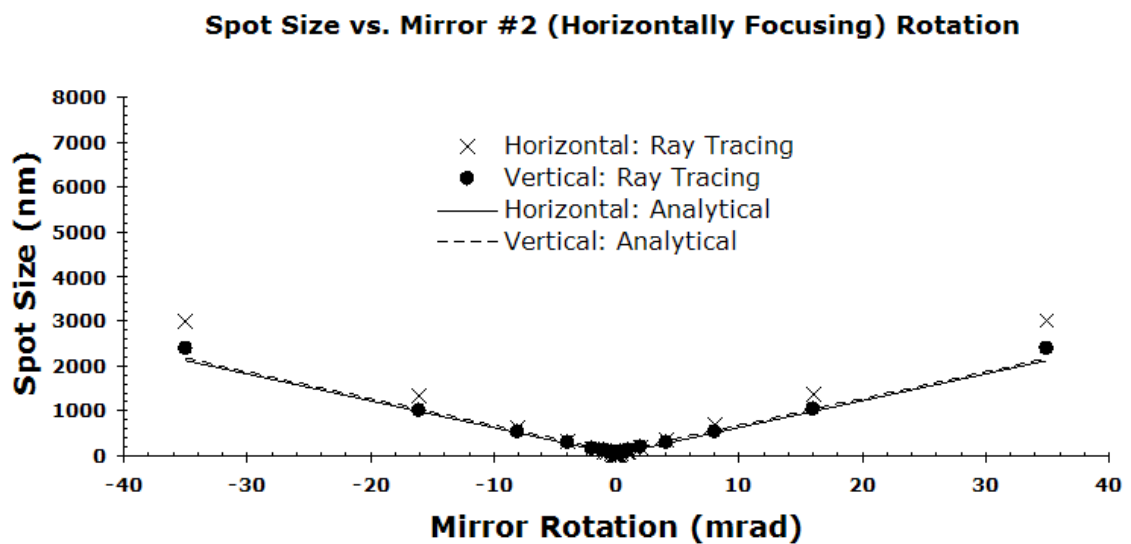


Figure 3.6. Image Sizes vs. Roll Misalignments of the Horizontally Focusing Mirror.

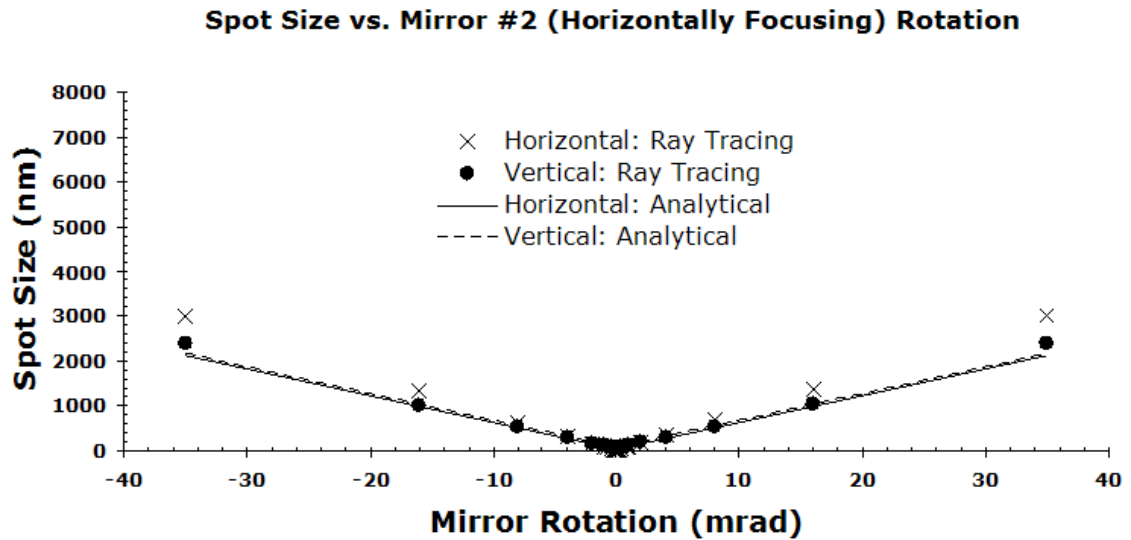
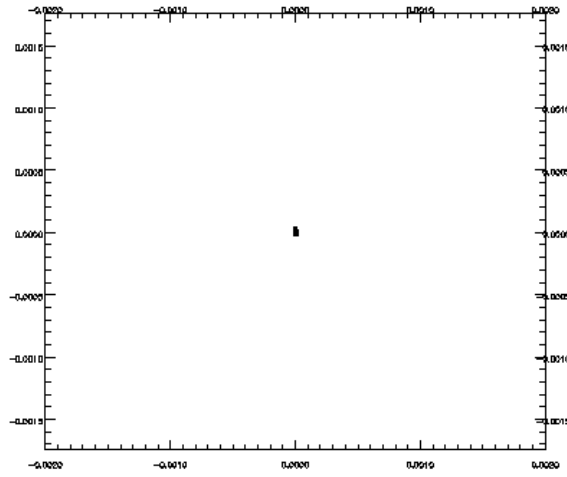
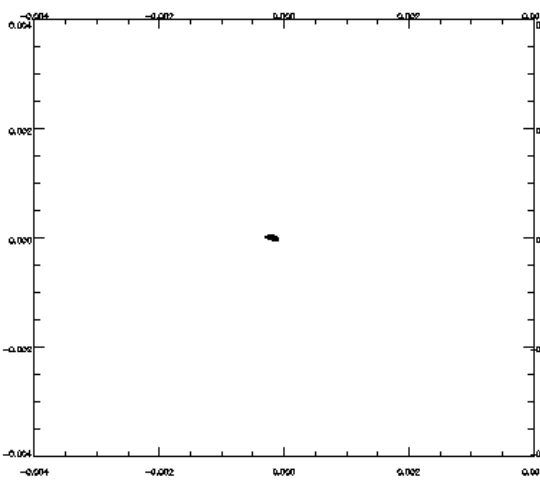


Figure 3.7. Image Sizes vs. Roll Misalignments of the Horizontally Focusing Mirror.

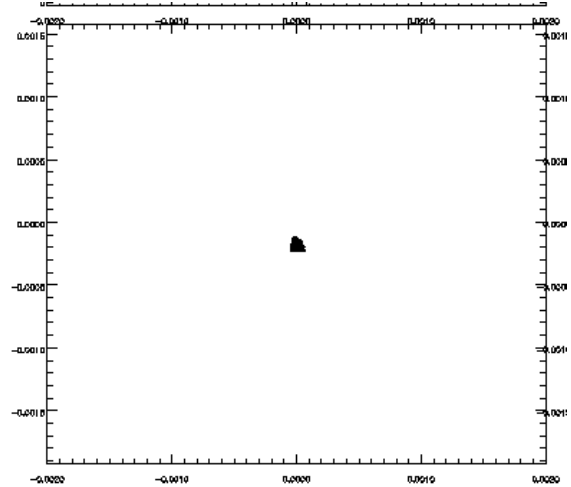
Enlargement of the focal spot exceeds 20% at mirror rotations of 0.1 mrad or more for the vertically focusing mirror and 0.2 mrad for the horizontally focusing mirror. Roll misalignment of the vertically focusing mirror (mirror #1) causes significant spot size enlargement in the horizontal direction because the incident beam on the horizontally focusing mirror (mirror #2) changes. As a result, the focal length of mirror #2 changes and the location of the focal spot to a different location in space, off the original beam path. When the image is observed at the original image plane, the beam is not completely focused. Rotation of the horizontally focusing mirror (mirror #2) does not change the angle of incidence of the x-ray beam to affect horizontal focusing and only causes spot size enlargement due to the location of the focal spot having been redirected off the original beam path. Figure 3.8 exemplifies the manner in which the spot is affected by the degree of roll misalignment. Each focal spot is imaged within a $4\ \mu\text{m} \times 4\ \mu\text{m}$ plot space.



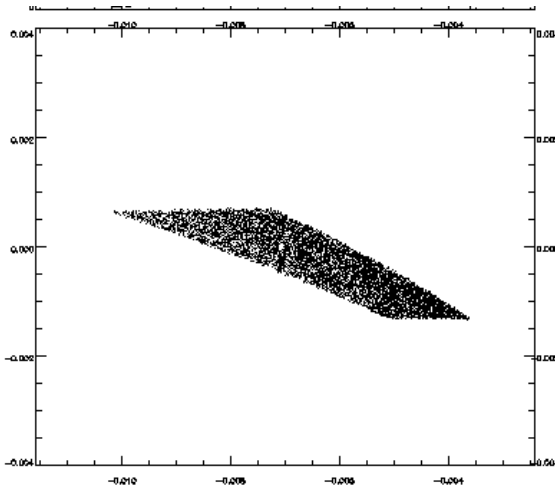
(a). Spot size of perfectly aligned mirror pair.



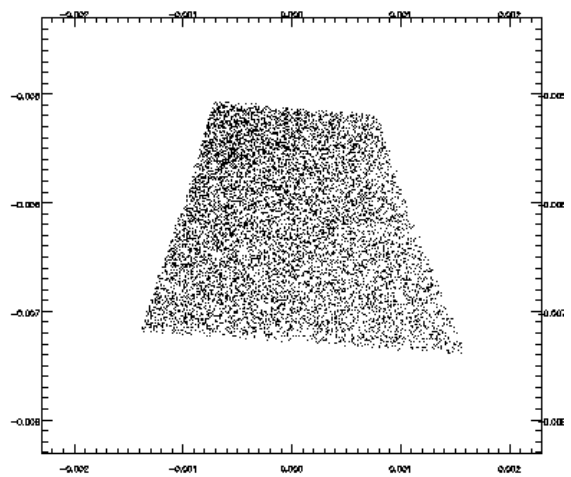
(b). 1 mrad roll of vertically focusing mirror.



(c). 1 mrad roll of horizontally focusing mirror.



(d). 35 mrad (2 deg.) roll of vertically focusing mirror.



(e). 35 mrad (2 deg.) roll of horizontally focusing mirror.

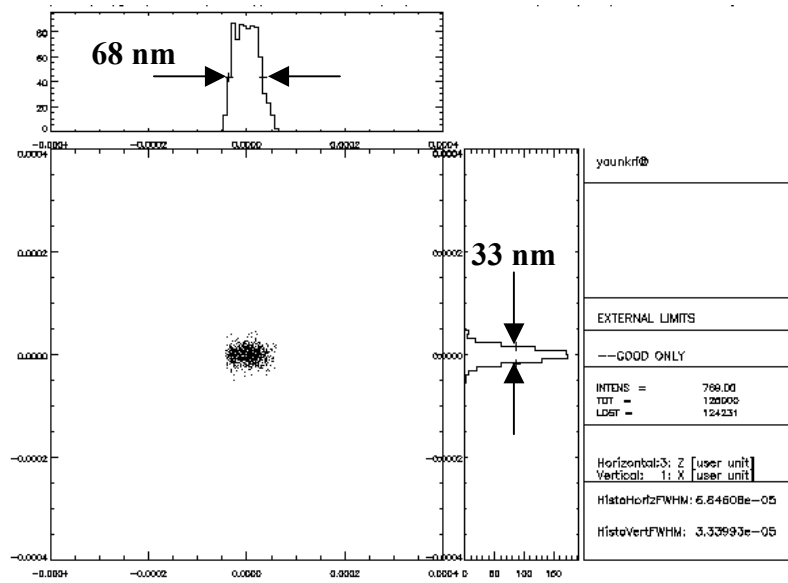
Figure 3.8 Ray-tracing Results for Various Types of Mirror Misalignment.

Ultimately, the alignment of the mirrors with respect to each other should be as orthogonal as possible. If the mirror mounting equipment cannot sufficiently align the two mirrors with respect to each other, then the alignment of the first mirror the x-ray beam encounters (the vertically focusing mirror in this instance) must be orthogonal with the incoming x-ray beam.

Ray-tracing simulations of a KB-mirror system have been demonstrated. Tolerancing of the alignment of each mirror has also been found to be very sensitive for nano-focusing. Roll misalignments of the mirrors greater than 0.1 mrad are found to enlarge the image by 20%. Such sensitivity to alignment is not an issue when aligning micro-focusing mirrors and raises the issue of choosing the right stage and alignment equipment to facilitate the necessary precision in alignment.

3.5 Shadow Roughness Modeling

Modeling the experimental layout begins by modeling the mirrors for the case where the mirrors are perfect and have no slope error. This insures that all parameters have been accounted for correctly and the resulting image agrees with expectations. For a source size of 100 μm (h) x 37.13 μm (v), a perfect image would be 72 nm full-width at half maximum (FWHM) in the horizontal and 33 nm FWHM in the vertical as shown in Figure 3.9.



Units are in mm.

Figure 3.19 SHADOW Simulated Focal Spot with Ideal KB Mirrors.

Next, the metrology results of the two mirrors are incorporated into the simulations. Both mirrors are measured via long-trace profiler (LTP) where the slopes of the mirrors are measured over their length. The vertically focusing mirror contained an overall slope error of $1.43 \mu\text{rad rms}$ while the horizontally focusing mirror had a slope error of $1.09 \mu\text{rad rms}$. Portions of each mirror however, contain areas where the slope error is within the range of 0.4 to $0.6 \mu\text{rad rms}$. The slope measurements were then integrated into heights and incorporated into the ray tracing simulation. In this case the measured heights are overlaid onto a flat mirror, resulting in an elliptical profile. It is also possible to overlay the height differences to an elliptical profile to simulate the measured mirror.

The vertically focusing mirror was simulated first with its measured profile while the horizontally focusing mirror is kept perfect. The vertically focusing mirror is then translated along the x-ray beam's path until the smallest vertical dimension of the spot is found. This positioning adjusts where the incident x-rays illuminate the mirror such that the area with the lowest *rms* slope area is illuminated. This process is aided by fitting the measured height profile to a curve fitting routine that determines a best-fit ellipse whose parameters would

suggest the optimum positioning and alignment of the mirror. In this case, the optimal positioning accounting for the slope errors suggested the mirror have an incident angle of 2.85 mrad and a focal length of 57 mm. Simulations were then performed with the mirror slightly translated along the beam's path to find the smallest vertical focal spot size as shown below in Figure 3.10.

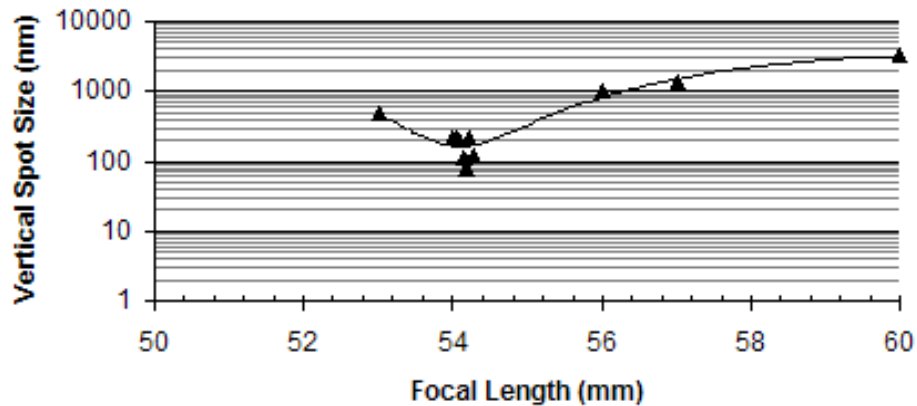


Figure 3.10. Vertical Spot Size vs. Mirror Position

Once the smallest vertical spot sizes were identified, the measured profile of the horizontally focusing mirror was incorporated into the simulation. The smallest focal spot with both measured profiles of both mirrors is found by leaving the vertically focusing mirror in its optimized position and then translating the horizontal mirror. The smallest focal spots found while positioning the mirrors is shown in Figure. 3.11.

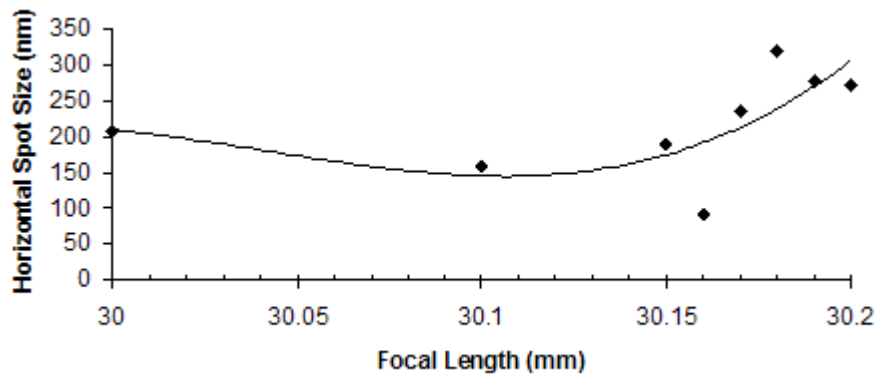


Figure 3.11. Horizontal Spot Size vs. Mirror Position.

Figure 3.12 shows that adjusting the mirrors' positions improves the resultant focal spot size closer to the design goal. It matches considerably well with experimental results achieved at the 34ID beamline (See Fig. 13 and 14). This is the smallest vertical spot size measured with a KB mirror at the APS. Table 3.3 shows the optimal positions and alignment of the mirrors on the beamline compared to those found via simulation. A spot size difference of 18% was observed in the vertical direction while a 9% difference was observed in the horizontal direction. The large differences in the results in the vertical direction are most likely due to measurements taken by the LTP. Measurements taken by this device are only a line measurement down the center of the optic along its length. This line measurement may not be the same path that the x-ray beam traversed during experiments. Additional LTP measurements would improve the difference between simulation and experiment.

Table 3.3 Simulated vs. Experimental Results.

	Vertical Mirror Focal Length (mm)	Horizontal Mirror Focal Length (mm)	Vertical Focal Spot Size (nm)	Horizontal Focal Spot Size (nm)
Beamline 34ID	61	30	95±10	85±10
SHADOW Simulation	54.19	30.16	77±10	93±10

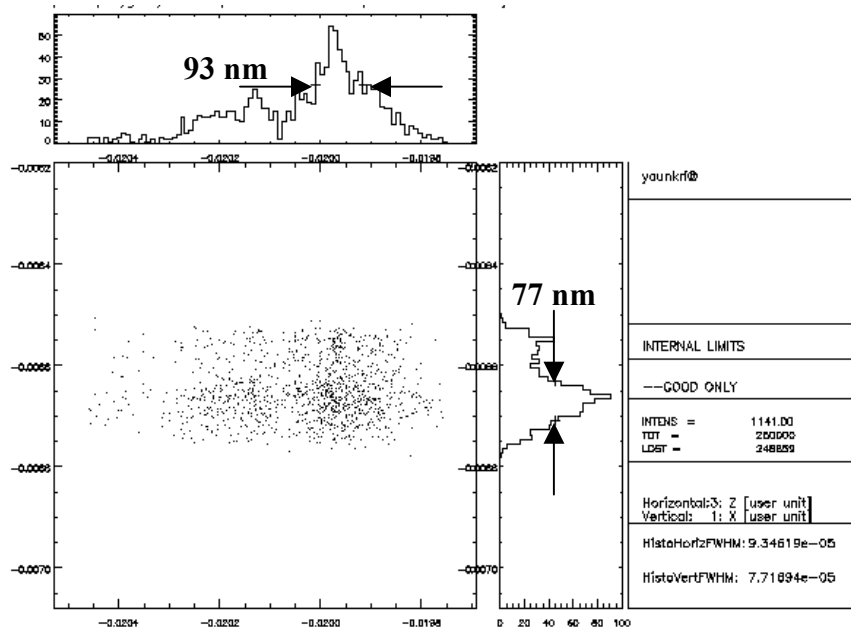


Figure 3.12. Smallest Simulated Focal Spot.

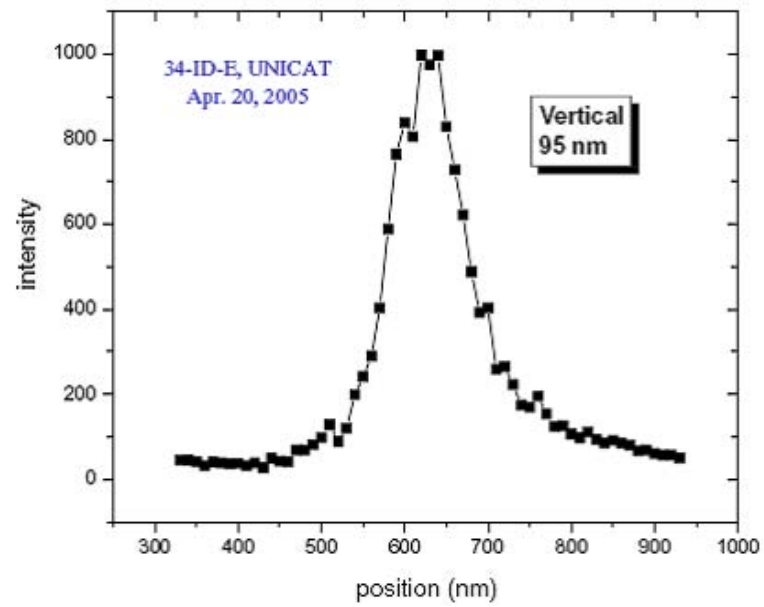


Figure 3.13. Smallest Vertical Focal Spot Size Measured at APS Beamline 34ID.

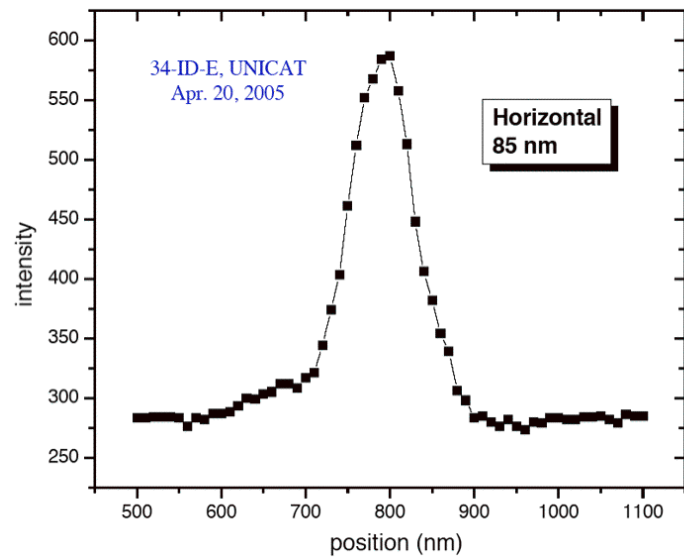


Figure 3.14. Smallest Horizontal Focal Spot Size Measured at APS Beamline 34ID.

CHAPTER 4

ALUMINUM COMPOUND REFRACTIVE X-RAY LENS

One method of fabricating CRLs is extrusion. Extrusion can be employed to produce, for example, aluminum CRLs for high-energy applications because many aluminum products are produced in this manner. Multiple lenses can be extruded in an array in a single run. This method is relatively cost effective compared to others methods of fabricating CRLs.

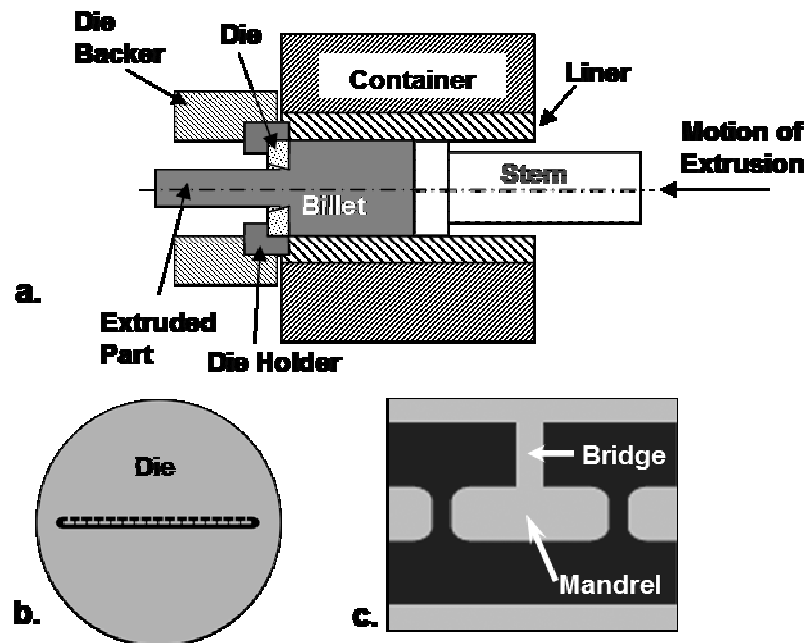
4.1 Design

The first CRL incorporating such extruded lens arrays was developed at the Advanced Photon Source [Khou02a]. Each array contained 15 lenses whose radius of curvature was 1 mm and wall thickness was 0.2 mm. The CRL itself consisted of 210 lenses. The CRL discussed here is the second generation with 240 lenses and pushes the limits of micro-extrusion by reducing the wall thickness and radius of curvature by a factor of 2. The wall thickness and radius of curvature are approximately 0.1 mm and 0.5 mm respectively. This wall thickness is the thinnest of such structures that have been extruded to date [Kraft04]. Further reducing the wall thickness may be possible by annealing and elongating the extruded lens arrays or by etching. Testing of the second generation is reported here.

4.2 Fabrication

For an energy range of 81keV, aluminum is employed because it allows sufficient x-rays to transmit the CRL at this energy. There are a number of methods of fabricating CRLs. In aluminum, hot micro-multi-port (MMP) [Guz01] extrusion offers an advantage over other available techniques, such as stamping, and machining; MMP extrusion allows multiple lenses to be extruded at once in arrays. This feature can allow for increased consistency between individual lenses and can fabricate many lens arrays inexpensively and accurately. The extrusion technique, however, can only fabricate one-dimensional focusing profiles. Paraboloidal and spherical lens arrays cannot be fabricated via extrusion.

A typical extrusion process involves a die, die holder, billet, container, liner, and stem [Laue81] (see Fig. 4.1a). A hot billet of material constrained in a container is forced through a die by the stem. Dies are machined with the negative profile of the part (lens array) to be fabricated into it (see Fig. 4.1b). In the case of hot MMP extrusion, mandrels bridged to the die form the shapes of the lens walls (see Fig. 4.1c). Material flows around the mandrels and bridges to form the lens walls; however, the outer wall segmented by the mandrels is joined together just before the array leaves the die. This process is called welding. Thermal shrinkage and welding are both accurately accounted for in die design such that the extruded part is not affected by the welding process.

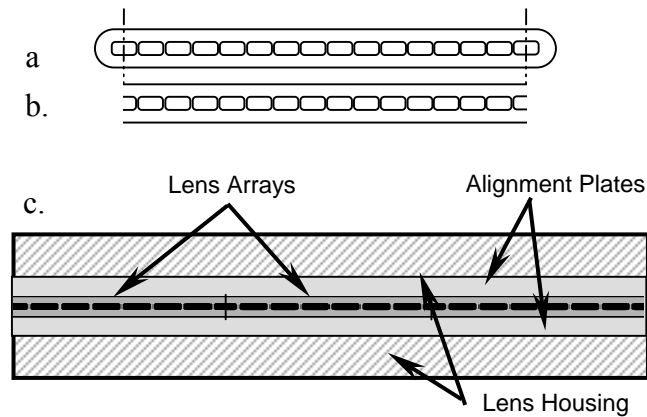


(a) a general extrusion layout, (b) a die plate used to extrude an array of parabolic lenses, and (c) the bridge and mandrel components of the die plate. The black portions of the die plate represent the area that is machined away.

Figure 4.1. Schematics of an Extrusion Apparatus

Once the lens arrays are extruded, annealed, elongated (to reduce wall thickness further) and cut, the round ends are removed via electro-discharge machining (EDM) (See Fig. 4.2a and 4.2b). They are then aligned side by side in between two alignment plates and fastened within an assembly housing (See Fig. 4.2c). The lens assembly or CRL is cut

diagonally such that the lens becomes a variable focus device: translating the CRL adjusts the number of lenses an incident beam passes through and in turn, the focal length (See Fig. 4.3).



(a.) Cross section of a single extruded array of lenses. (b.) The ends are removed via EDM and each array is (c) aligned side-by-side with the next until the desired number of lenses is reached.

Figure 4.2. Fabrication of the Aluminum CRL Array.

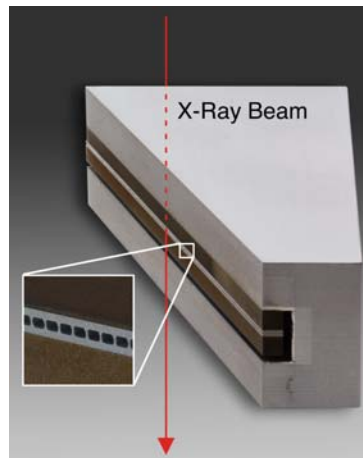
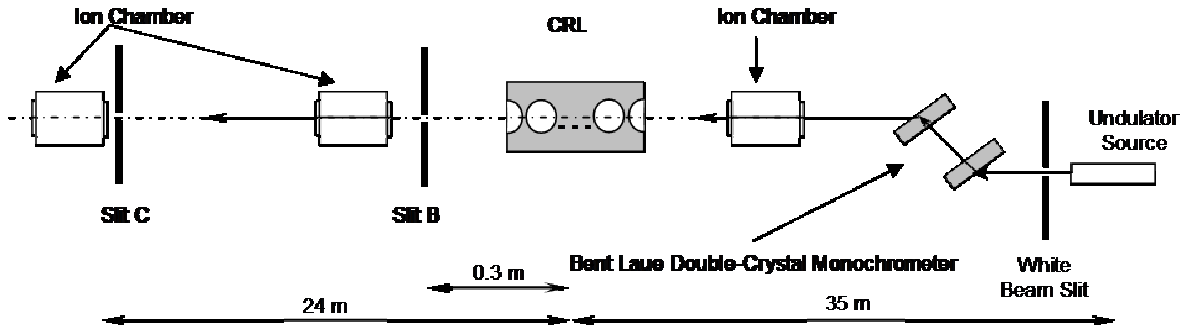


Figure 4.3 Photo of Manufactured CRL.

4.3 Testing

The CRL was tested at the APS 1-ID beamline with a monochromatic 81 keV undulator beam to observe vertical collimation and focusing. The beamline layout is shown in Figure 4.4. The beam from an undulator source was monochromatized by a bent-Laue double-crystal monochromator and passed through the CRL located 35 m from the source. The transmitted beam was then vertically scanned at two locations to determine its size: at slit B, 0.3 m downstream of the CRL, and at slit C, 24 m downstream. Initial scans at both locations

were taken without the CRL in place. The following scans were performed as the CRL was translated horizontally allowing the beam to pass through an increasing number of lenses. The same procedure was used to evaluate the first-generation CRL [Khou02b].



The incident beam is conditioned by a white beam slit and bent Laue double-crystal monochromator before passing through the lens. Once the beam passes through the CRL, it is measured at two slit locations; the first 0.3 m downstream from the lens and the second 24 m downstream from the lens. NOT TO SCALE

Figure 4.4. Schematic of Aluminum CRL Beamline Layout.

Beam profiles at slit B show the effect of absorption on the transmitted beam as the number of lenses increase. Absorption is characterized by the percentage of x-rays absorbed by a given number of lens walls. The amount of x-rays transmitted is therefore the percentage of x-rays that transmit through a given number of lens walls and is expressed by Lambert-Beer's law Equation 4.1.

$$T = \exp(-\mu Nt), \quad (4.1)$$

μ is the linear absorption coefficient, N is the number of lenses, and t is the thickness of the each lens wall. The transmission is a function of the lens thickness at a given point along its profile. As the thickness increases away from the optical axis, transmission decreases. Transmission of the lens was measured at slit B and was in good agreement with calculations as shown below in Figure 4.5.

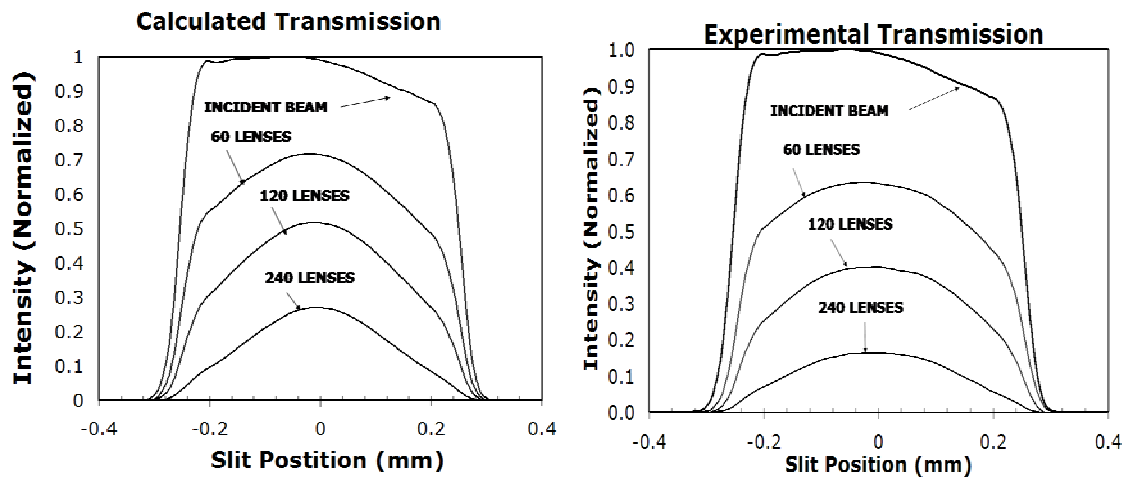


Figure 4.5. Calculated and Experimental Transmission Profiles.

The focused beam profiles measured at slit C experienced a double focus, or two concentrated intensity peaks (See Fig. 4.6). As the CRL was adjusted to increase the number of lenses, the two peaks converged to form one, however, without any intensity gain. Intensity gain is a measure of the increase in peak intensity of a focused beam profile compared to an unfocused beam profile under the same condition. Despite the absence in gain, focusing did occur since the beam profiles experienced an increase in peak intensities at slit C compared to slit B.

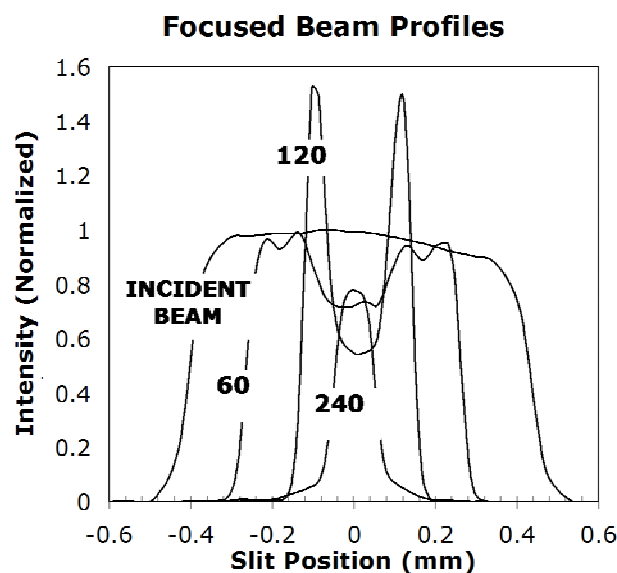


Figure 4.6. Measured and Normalized Intensity Profiles of the X-ray Beam at the Image Distance.

The measured beam profiles were then used to compare the CRL's performance with expected performance. Eighty-six (86) lenses were expected to collimate the 81 keV beam for the given beamline layout, assuming no absorption is taking place. Including absorption, 90 lenses would be needed. This calculation is exemplified by the intersection of the two curves representing the expected beam size at the two slit locations as a function of the number of lenses the incident beam passes through (See Fig. 4.7). The reduction in beam size at slit B, 0.3 m downstream from the lens, corresponds to the non-uniform thickness of the lens walls, resulting in increased absorption on the periphery of the beam, whereas, at slit C, the reduction in beam size is due to both absorption and focusing. Two hundred and twelve (212) lenses were expected to focus the incident beam at 24 m. This is represented by the minima of the curve showing the expected beam size at 24 m. In experiment, collimation was achieved when the measured FWHM of the x-ray beam profile at slit B 0.3 m downstream from the lens was equal to that at slit C 24 m downstream. For those profiles with double peaks, the width of the entire profile was measured at half the maximum intensity, ignoring individual peak widths. Including this assumption, collimation occurred at 75 lenses.

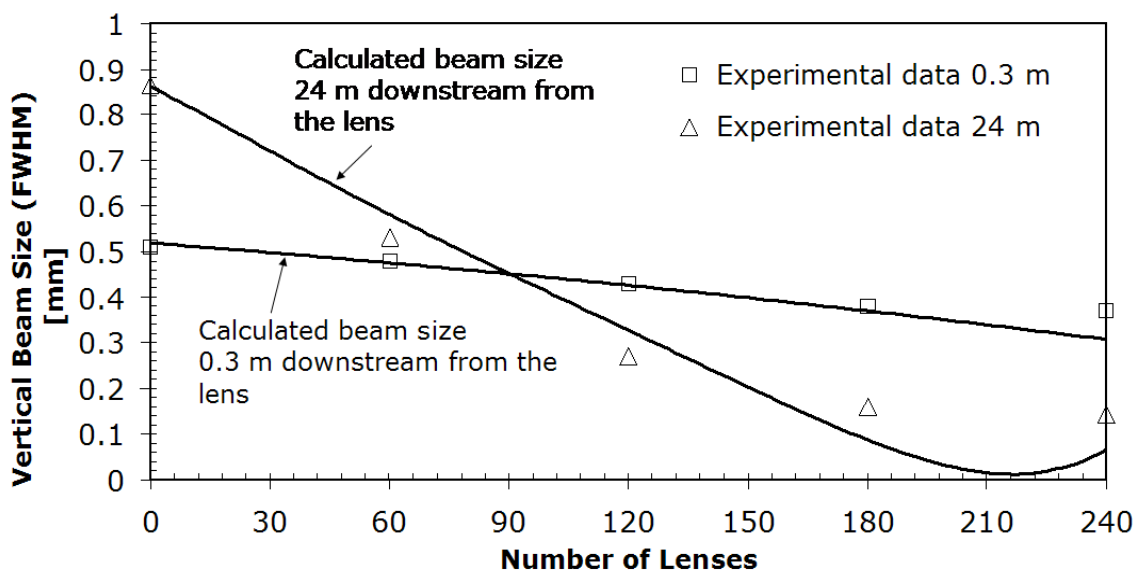


Figure 4.7. Vertical Beam Size (FWHM) of the X-ray Beam Downstream from the Lens.

The CRL's focusing did not meet expectations. Calculations predicted a gain of 28 with 212 lenses [Snig98] as shown using Equation 4.2;

$$G = \frac{A_{eff}}{\sigma_s} \left(\frac{S}{S'} + 1 \right) \exp(-\mu Nd), \quad (4.2)$$

where the effective aperture (See Eqn. 4.3) of the lens A_{eff} is limited by absorption. Beyond this aperture, the transmission falls below e^{-1} and is ignored. The Gaussian source size is σ_s , S is the source distance, and S' is the image distance.

$$A_{eff} = 2 \left(\frac{2R}{N\mu} \right)^{\frac{1}{2}} \quad (4.3)$$

Had the lens only been affected by its effective aperture and diffraction-limited resolution, the gain would be approximately 1600 as given by Equation 4.4:

$$G = \frac{A_{eff}^2}{\lambda S'} \left(1 + \frac{S'}{S} \right). \quad (4.4)$$

The double focus is the cause for the poor gain and may be the result of the lenses deviating from a parabolic profile. Deformation during production is the likely cause, because the extruded arrays were coiled before being annealed, stretched, and cut into strips of the desired lengths. This coiling may have deformed the lens walls in such a manner that they had become biased in one of two directions such that two foci were created. A comparison between the lens wall cross section of the initial lenses and the current lenses (See Fig.4.8) relays the differences between the two generations.

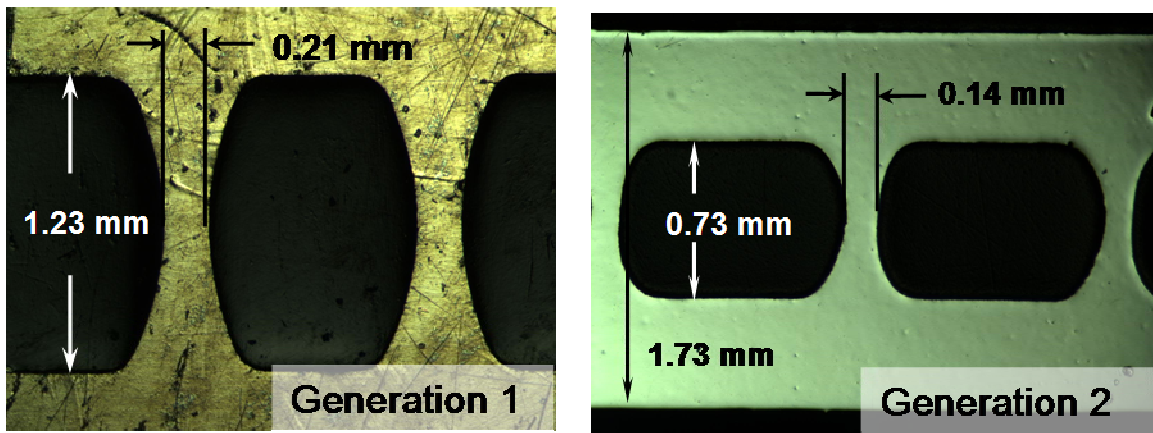


Figure 4.8. Comparison of First (left) and Second (right) Generation Al CRL Profiles.

Of the current lens arrays whose profiles were compared to the specified parabolic curve, only 30% of the profiles were acceptable. The difference between the resultant profiles of the two generations is that the first-generation lenses were not coiled after extrusion. This difference in processing is attributed to the appearance of the double focus using the current lens. Another possibility is misalignment between the extruded strips as they were laid side by side between alignment plates. A third generation of lenses is being produced that will not be coiled in order to confirm the cause of the deformation.

The fabrication and testing of a second-generation variable-focus compound refractive x-ray lens is summarized. The current x-ray lens showed the possibility to further push the capabilities of extrusion as a means of fabrication by decreasing the lens wall thickness by a factor of two from 0.2 mm to 0.1 mm. The radius of curvature of the lens was also reduced by a factor of two from 1 mm to 0.5 mm. An expected gain of 28 was hampered by what is believed to be the deformation of the lens walls during the post-production coiling process. Nevertheless, extrusion shows promise as a means of fabricating inexpensive x-ray lenses. A third generation of extruded lens arrays is being produced to resolve the cause of the deformation of the lens walls.

CHAPTER 5

LITHIUM COMPOUND REFRACTIVE X-RAY LENS

Although compound refractive lenses comprised of aluminum [Snig96], beryllium, epoxies, Kapton [Pie00], etc. have been fabricated in the past ten years, lithium remains one of the most suitable and exciting material for this application. It is the lightest metal having an atomic number of three and would allow the greatest transmission of x-rays for a given thickness. It is the material of choice for x-ray lenses in the moderate (2-40 keV) x-ray energy range because of its high transmission, as well as its high refractive index decrement δ (see Eqn. 2.2). This means that lens-for-lens; lithium focuses x-rays more than other elemental materials in this range and absorbs the least amount of x-rays. Lithium hydride has the potential to surpass lithium with regard to absorption but is extremely reactive, brittle and manifests itself primarily as a salt like powder. The short focal lengths afforded by lithium CRLs however, allow their use not only on synchrotron x-ray beams, but potentially on laboratory-based x-ray systems in widespread use worldwide.

The major obstacle to fabricating suitable lithium lenses is that lithium reacts strongly and rapidly with moisture and to a lesser extent with oxygen and nitrogen. Thus, it is necessary to conduct lithium work in a dry environment and preferably in an inert atmosphere (e.g. argon or helium). This has impeded the use of lithium as x-ray lenses because it has developed a stigma of being a highly reactive and tough material to handle. Despite this, a number of lithium CRLs have been fabricated.

The first successfully tested lithium CRL [Duf01] utilized a multi-prism or alligator jaw geometry that was first proposed by Cederstrom [Ced02]. This geometry consists of two strips each having a given number of triangular teeth that act as jaws and may open and close to adjust the focal length. This lithium lens achieved a gain of 3 compared to a theoretical expectation of 4.5 at 10 keV. The shortfall in gain was attributed to the poor surface figure

and finish of the die tooling used to press the saw tooth profile into the lithium strips. Lithium CRLs containing lenslets with parabolic profiles were then fabricated with radii of curvature at the tip equal to 1 mm [Crem00]. A measured gain of 18.9 was obtained despite a theoretical expectation of 47.7 at 8 keV. Again the lower value of measured gain was attributed to figure and finish of the pressed lithium lenslets. The latest reported lithium CRLs with parabolic lenslet profiles had radii of curvature at the tip equal to 0.263 mm and obtained a measured gain of 20 to 40 compared to a theoretical gain of 259 [Per04]. A consistent theme with the lithium CRLs fabricated to date is that the figure and finish of the lenslets were not sufficiently adequate to allow the lenses to perform to the theoretical expectations. In addition, no metrology on the lithium lenses has been performed to date. Refinement of the fabrication techniques of lithium CRLs and characterization of the lens surfaces is absolutely necessary to improve the performance of lithium CRLs.

5.1 Material Properties of Lithium Metal

Pure lithium is an alkali metal with a body-centered cubic (BCC) crystal structure and appears white and silvery in color. It is very malleable and typically exhibits a dull finish. General properties of lithium metal are listed below in Table 5.1 [Jep78] *[Mat05] ‡[Tar03]. A plot of lithium's mechanical behavior with respect to stress and strain at various strain rates is shown below in Figure 5.1 [Tar03].

Table 5.1 General Material Properties of Lithium Metal.

Material Property	Value
Atomic Number	3
Atomic Weight	6.941 a.m.u.
Density*	0.53 g/cc
Cubic Edge Length of a Unit Cell	3.51 Å
Yield Strength [†]	1.10 MPa
Young's Modulus [‡]	7.8 GPa
Ultimate Tensile Strength [†]	2.28 MPa
Melting Point	180.54°C
Boiling Point	1347°C
Heat of Vaporization	4680 cal/g
Heat of Fusion	103.2 cal/g
Heat Capacity*	3.305 J/g°C
Thermal Conductivity*	71.2 W/mK
Coefficient of Thermal Expansion*	56 $\mu\text{m}/\text{m}^\circ\text{C}$
Electrical Resistivity*	8.4eE6 ohm-cm

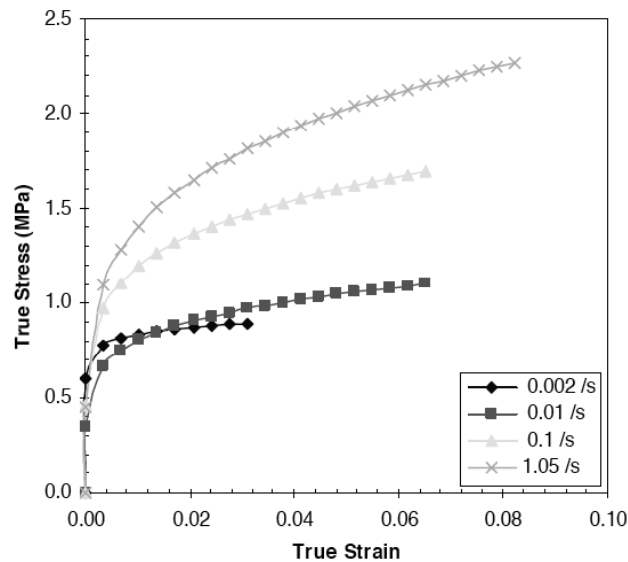


Figure 5.1. True Stress vs. True Strain of Lithium.

Lithium has the potential to be the most suitable material to use as a CRL because it refracts x-rays a relatively large amount and is very transparent to x-rays as shown in Figure 5.2 [Rio98]. This makes lithium the closest analogy to glass with respect to optical properties in the visible regime.

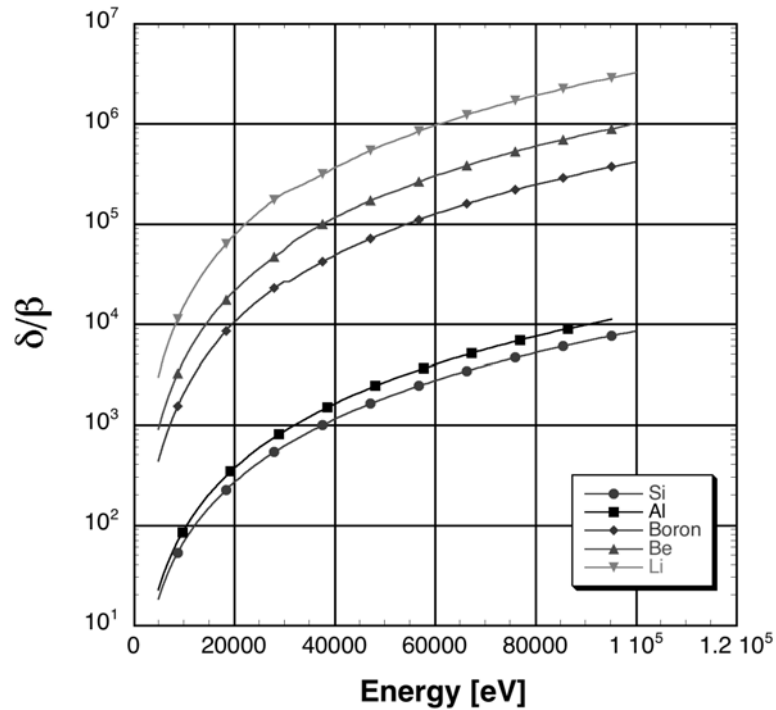


Figure 5.2. Refractive Index Decrement over Absorption vs. Energy.

Lithium is the least reactive of the alkali metals but its reactivity is temperature dependent; as the temperature increases, its reactivity also increases. Figure 5.3 shows lithium's reactivity with the typical constituents present in atmospheric conditions such as water, hydrogen, oxygen, and nitrogen [Jep78].

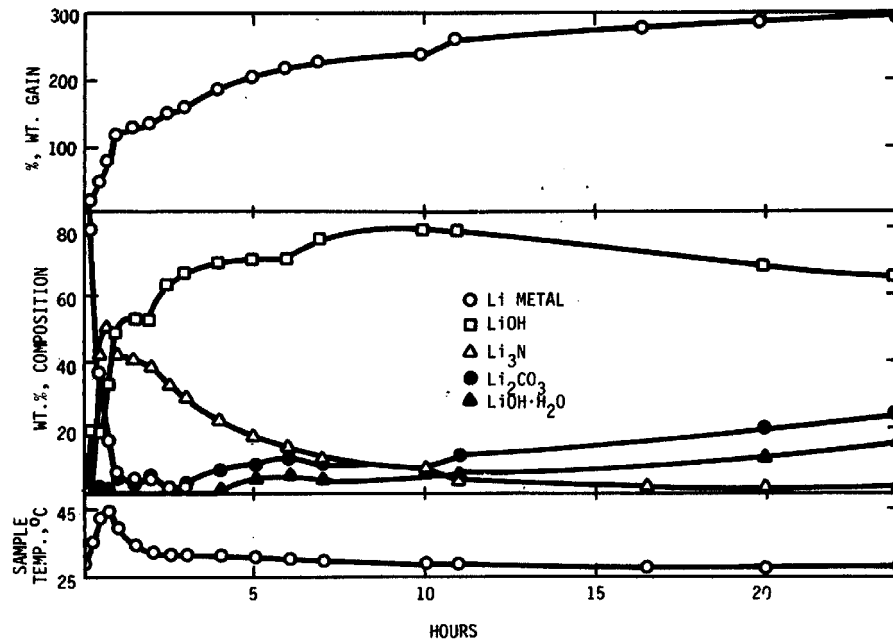


Figure 5.3. Reactivity of Lithium with Air.

The products of the reactions appear as coatings on the surface of the lithium metal (See Fig. 5.4) [Jep78]. These products seriously degrade the optical properties a lithium lens and make the production of lenses under normal conditions impossible. This generates the need to fabricate and maintain lithium lenses in an inert environment. Helium and argon filled glove boxes are typically employed when handling lithium, although it is also sufficient to handle lithium in a dryroom environment where the humidity in the air is kept to a minimum. By limiting the amount of moisture present in the air, lithium's reactivity to the other constituents in air such as hydrogen, oxygen and nitrogen is severely retarded [Jep78].

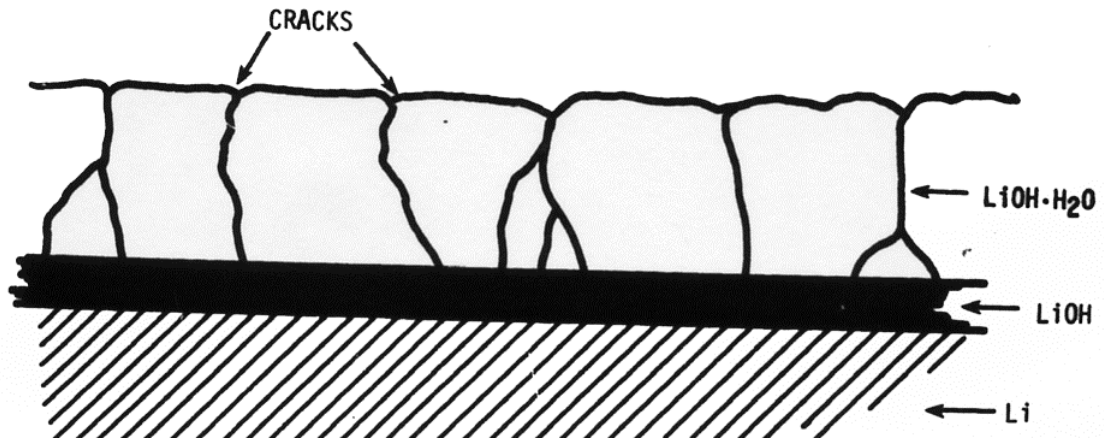


Figure 5.4. Schematic of the Cross-section of Lithium Reaction Products.

5.2 Design of a Lithium CRL

The design of a lithium compound refractive lens has to account for four major considerations; fabrication techniques that best accommodate lithium's properties, the figure and finish of the lenslet profiles, the alignment of the lenslets, and the containment of the lens unit as a whole to prevent the degradation of the pure lithium.

Lithium's reactivity and malleability limits the techniques that can be employed to fabricate lenslets with a given profile. Conventional machining is not feasible because lithium is too soft and the friction between the lithium and the machining tool would increase the temperature of the lithium causing it to become more reactive. Casting and extrusion also involves heating lithium. In addition, lithium tends to adhere to dies and tooling, requiring

lubricants that would not leave any films or residue that would react with the lithium or simply cause added absorption of x-rays. Techniques that have and may be proven feasible include pressing, and punching, however, punching is less favorable because it produces lenses that are capable of one dimensional focusing only.

In this light, pressing is the simplest and most cost effective means of producing high quality lenslets given lithium's properties. Pressing lithium would require a small press fixture that can fit easily into a glove box and the lithium need not be heated to induce flow around the tooling that is pressed into the lithium. The press would be fitted with a high precision die set that would generate consistency between presses and would allow for tight tolerances and alignment of each lenslet that is pressed. Tooling can then be mounted into the die set to perform the actual forming of the lithium. The advantage of such a design is that the tooling itself can be interchangeable and allow for replacements or different shapes and dimensions to be used. Figure 5.5 below shows a picture of the SCHMIDT manual pressing unit currently employed to fabricate lithium lenslets at Argonne National Laboratory. Affixed to the press is a FIBRO die set with ball bearing guides to increase accuracy and repeatability of the die set.



Figure 5.5. Photo of Pressing Fixture Employed to Press Lithium Lenslets.

The figure and finish of a CRL determines the resolution and maximum focusing capabilities of the device as an optic. The term figure is meant to describe how accurately the shape of the fabricated lenslet profiles match the design ideal, while finish is intended to describe the surface roughness of the lens. As is the case for optics that operate in the visible light regime, a scratched and warped lens would distort and blur the resulting image produced by the optic, this is no different in the x-ray regime. The ultimate intent for CRLs is to produce the smallest x-ray beam (microns or less in size) with the highest intensity possible, and implies that the figure and finish of the lenses be as accurate and smooth as technologically feasible. In the case of lithium, it is inherently a material with a rather dull surface finish and cannot be polished by conventional means because of its malleability.

By employing pressing as the fabrication technique, it is possible to impress the lithium with a very accurate spherical or parabolic indenter with exceptional surface roughness characteristics and impose the figure and finish of the indenter onto the lithium. Spherical indenters employed in the die press fixture described above are Rockwell hardness indenters loaded with grade 10 440c stainless steel 1/16" diameter balls (See Fig. 5.6). Grade 10 precision balls are specified to be accurate in diameter and roughness average Ra to 0.25 μm (1 μin). Prototype parabolic indenters with tip radii of 0.1 mm have also been fabricated from 440c stainless steel with a CNC lathe unit at IIT. As turned, the parabolic pieces have a surface roughness of approximately 1.6 μm (64 μin) and required further processing to improve their surface finish. Mechanical polishing was attempted although polishing in this manner can alter the shape of the machined piece and was deemed unreliable. Electropolishing was then viewed as the best means for achieving the best surface finish on the parabolic tips. With this in mind, several attempts at electropolishing the tips were made with published recipes [Van02] for stainless steels without success. As a result the indenters were outsourced for electropolishing with proprietary techniques. Unfortunately,

electropolishing of 440c stainless steel can only improve the surface roughness by a factor of two and a roughness of $(0.8 \mu\text{m}) 32 \mu\text{in}$ was achieved. Figure 5.7 shows the difference between an electropolished part and a part as turned on a lathe. The best surface finishes that can be achieved with electropolishing of stainless steels are done so with 300 series alloys and is described next.



Figure 5.6 Rockwell Hardness Indenter with Ball Tip.

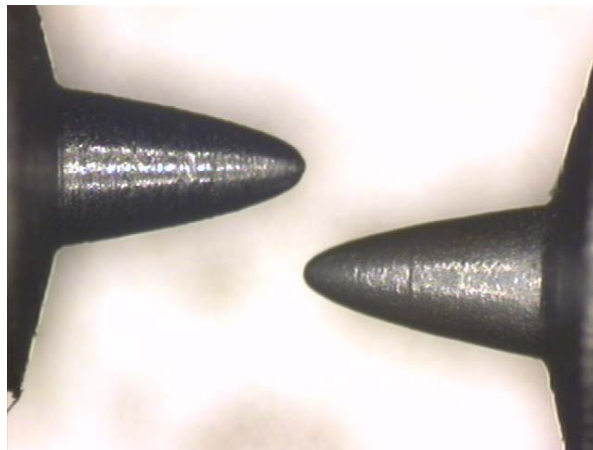


Figure 5.7. Unpolished (left) and Electropolished (right) 440c Stainless Steel Parabolic Indenters.

Additional parabolic indenters were fabricated from 316 stainless steel and were successfully electropolished using a perchloric ethyl alcohol solution. The results of electropolishing 316 stainless were far better than those for 440c as shown in Figure 5.8. Etching is evident at the base of the indenter profile. This is caused by overexposure to the polishing solution or a raise in temperature in the solution. This is the first trial in

electropolishing 316 stainless steel and better results would be achieved if the polishing were performed by an outfit that specializes in electropolishing. Many of the solutions, conditions, and techniques employed in electropolishing materials are patented and trade secrets, making it difficult to achieve optimal results in the first attempt.

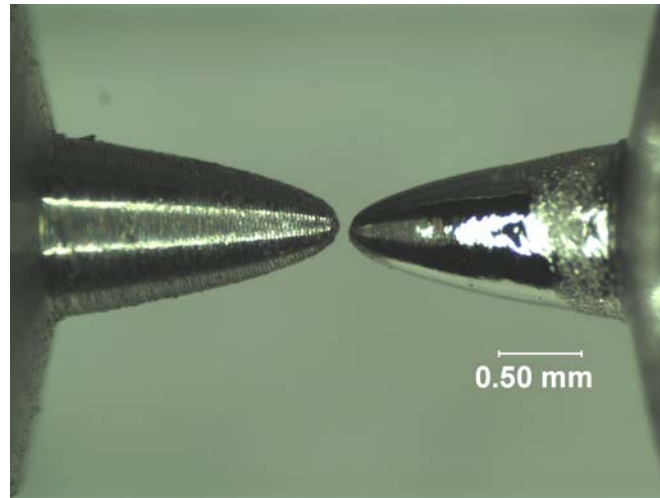


Figure 5.8. Unpolished (left) and Electropolished (right) 316 Stainless Steel Parabolic Indenters.

In addition to figure and finish, alignment is a serious consideration and can also affect the performance of a CRL. Misalignment can cause blurring of the focal spot because all lenses are not focusing to the same point in space as well as increased absorption. The increase in absorption would come about because an incident beam having a Gaussian intensity profile would no longer have its brightest portion (the center) passing through the minimum wall thickness of the lenses. Pantell and associates released an interesting analytical investigation of the effects of surface roughness and misalignment of lenslets within a CRL [Pan01]. The analysis concluded that misalignment of up to $25\ \mu\text{m}$ can be tolerated and would cause a 2.5% increase in the lens wall thickness that the incident x-ray beam would have to traverse through. The tolerance for surface roughness was concluded to be limited to an amount such that the phase shift of the x-ray beam was not altered by an amount greater than $\pm\pi/4$. These are relatively large tolerances compared to other x-ray optics and allow greater ease in manufacturing tolerances.

Alignment in the design employed is maintained throughout using dowel pins and alignment rods that pass through holes in the cartridge units that contain the lithium to be pressed. The lithium cartridge units (See Fig. 5.9) serve as protective containers that hold the lithium in place during pressing and maintain alignment when they are arranged in series. Dowel pins that fit through the holes in the cartridge unit are pressed into the die set tooling to act as placement guides for the cartridge units such that the indenters press into lithium in the same location consistently with respect to the cartridge unit. Once the desired number of lenses are arranged in series with the two alignment rods threaded through the holes in the cartridge units, the lens array is then braced on both ends by caps which in turn will have three support rods threaded on both ends that span the length of the array clamping it together between the caps allowing for the entire unit to act as a single rigid body (See Fig. 5.10). Nuts would be tightened on both ends of the rods securing the array in its alignment. The entire unit is then able to be secured in place within an air tight housing with beryllium windows on both ends to allow the x-ray beam to traverse through the lens array (See Fig. 5.11). The housing unit itself is comprised of vacuum components and can be evacuated or backfilled with helium to preserve the state of the lithium during its service life. A glass view port is located at the central portion of the housing to view the conditions within via strips of lithium getter material. The lithium getter material is wrapped outside the lenslet cartridges such that if there is moisture or air present within the housing, the lithium getter material will be the first material to react and will indicate the presence of contaminants. All engineering drawings associated with the design of the lithium lenslets are included in Appendix A for further detail.



Figure 5.9. Lithium Lenslet Cartridge Unit.

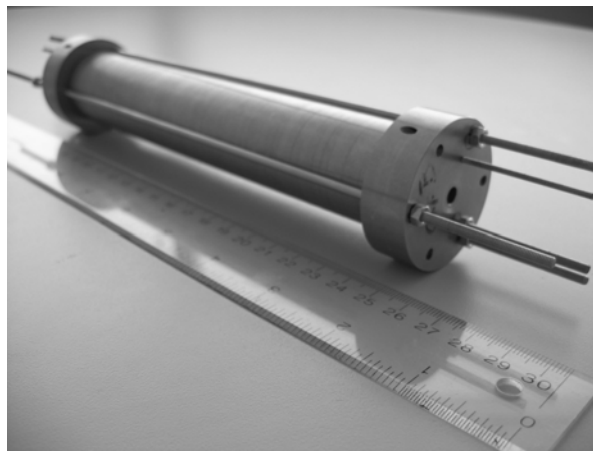


Figure 5.10. Photo of the Lens Array Assembly.

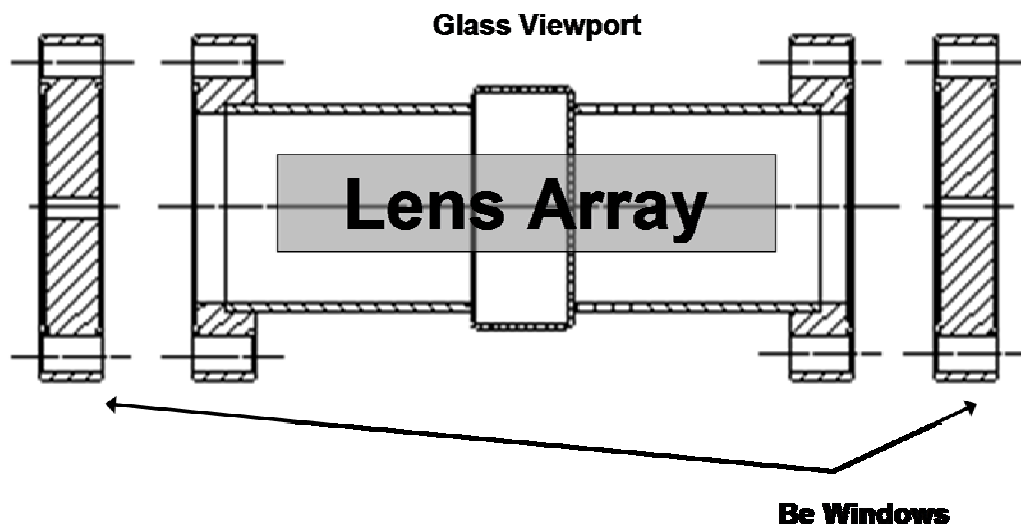


Figure 5.11. Design Schematic of Lithium Lens Housing Unit.

5.3 Fabrication of Lenslets

The fabrication of the lithium lenslets with the equipment described above is outlined in the procedure below. Supplementary material regarding the safe handling, storage and disposal of lithium is provided in Appendix B.

1. Once the necessary personal protective equipment is assembled as outlined in appendix B they should be worn.
2. Place a rubber stop in between the die plates to prevent the die plates from accidentally coming together.
3. Prepare all equipment associated with the press. If one is setting up an experiment for the first time, two people should be present to ensure everything is performed safely and smoothly:
 - a. Affix the miniature die set to the press by screwing in the bottom $\frac{1}{2}$ " bolt (bolt with a head) from below the base of the press into the bottom die plate until nearly finger tight. There should be some play to allow for alignment adjustments.
 - b. Screw in the top $\frac{1}{2}$ " bolt (headless) at least $\frac{1}{2}$ " into the top die plate and insert the top of the bolt into the ram of the press.
 - c. Gently tighten the setscrew in the ram of the press to affix the top die plate in place. Make sure that as you tighten, the alignment of the die plates is not affected. Misalignment restricts the top die plate from moving up and down freely.
 - d. Likewise, for the bottom bolt, gently tighten it until the die plate is securely aligned and attached to the press.
4. Install and align the press fixtures:
 - a. Insert dowel pins into their respective holes in the bottom press fixture. The bottom press fixture is characterized by having only two holes drilled into its face.

- b. Install the bottom press fixture to the bottom die plate. Align the fixture such that the setscrew holding the indenter in place is facing the forward toward the operator. Allow some play for alignment.
 - c. Install the top press fixture to the top die plate. The top fixture is characterized by having three holes drilled on its face. Do not tighten the machine screws. Allow some play for alignment.
 - d. Remove the rubber stop and engage the lever to bring the die plates close together, just enough so that the dowel pins just enter the top fixture bringing the two pieces in alignment.
 - e. Tighten all the machine screws on the fixtures until they are secure.
5. Go to a well-ventilated area and inspect the lithium container for signs of pressure build-up before opening.
 - a. If a hissing sound is heard or the lithium ignites, call 911.
 6. Place all needed materials in the work area within the glove box or dry room such as Lith-X, a spill tray, tongs, and all other necessary equipment.
 7. Place the container of lithium in the work area and place the lithium on the spill tray.
 8. Use a round punch to cut disks (11 mm dia.) of lithium from the bulk lithium foil.
 9. The lithium disks are then placed in to a stainless steel cartridge unit to hold the lithium disk in place and to minimize the amount of lithium in contact with the pressing fixtures.
 10. A small amount of lubricant such as mineral oil, hexane, or nonane is applied via swab.
 11. A cartridge unit carrying a lithium disk is placed on the bottom press fixture by sliding the aligning pins through the holes of the lens cartridge.
 12. The rubber die press stop is removed to allow the die plates to move freely and the lever on the press is used to draw the die plates close together and press spherical indentations into the lithium disks.

13. Once the lithium disk is pressed, the cartridge unit is removed from the pressing fixture and placed in a housing unit or stored in a sealed container.
14. The pressed lithium disk may also be chemically polished with diethyl ketone by applying a small amount with a swab and allowing the ketone to remain on the lithium for no more than a minute before removing it with a swab and disposing of the swab according to the methods outlined in the MSDS for diethyl ketone.
15. Any unused lithium is to be stored in the designated storage area at the end of the day.
16. Follow the disposal methods outlined in Appendix B for scrap lithium.

5.4 Characterization of Lithium Lenslet Profiles

Once the lithium lenslets are impressed with their bi-concave profiles, the figure and finish of the profiles need to be measured to quantify their quality with respect to the design ideal. Logistical constraints involved in the performing metrology on the lenslets exist because the necessary equipment such as white light interferometers and stylus profilometers are not located within the glove boxes or dryrooms where the lithium lenslets are fabricated. The lithium lenslets would then have to be transported in a controlled environment capsule and measured within a capsule containing the measurement equipment. An alternative is to measure the profiles by proxy via a negative cast of the lenslet profiles. The indentations on the foil are filled with a polymethylsiloxane blend that cures and forms a negative cast replica of the indentations that in turn can be measured under normal environmental conditions. The method of measurement employed to characterize the figure and finish of the replicated lenslet profiles was a 3D Optical Profiler (White light interferometer).

The 3D optical profiler used was an ADE Phase Shift MicroXAM unit. The optical profiler operates similarly to a conventional optical microscope with the exception of the objective lenses and the software used to process the images received from the objective. A white light interferometer takes advantage of the wave nature of light and uses interference

fringes to measure heights on a surface. It consists of the following components, a camera, a light source, objective, beam splitter and reference mirror (See Fig. 5.12) [Zec04]. Light from the source passes through the objective and reaches the beam splitter where a portion of the beam is reflected to the reference mirror and the rest reaches the sample. Light reflected back from both the sample and reference mirror is recombined at the objective where fringe patterns form and are recorded by the camera and interpreted. The fringes represent the optical path difference between the interfering waves from the sample and reference mirror. The microscope interprets the fringes as it focuses through a given scan height. The difference in time for one point to come into focus with respect to another determines the height difference between the two points.

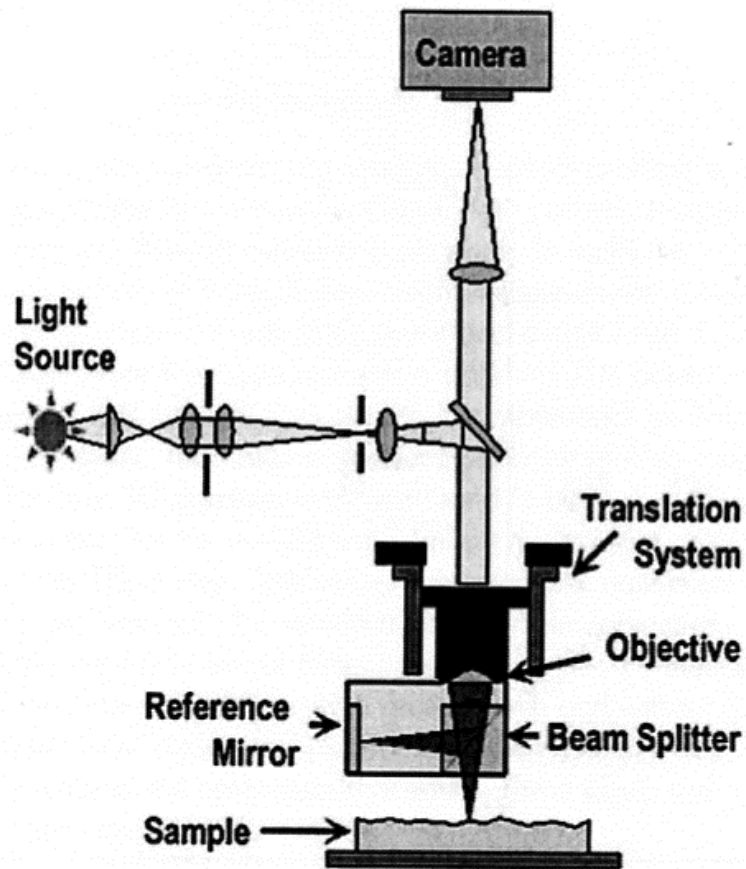


Figure 5.12 Schematic Diagram of a White Light Interferometer.

This instrument is capable of 0.1 nm resolution although is limited in interpreting high slopes on the order of 1.2 to 22.6 degrees [Carp05]. Measurement of the spherical lens

indenter and replicated lens profiles were measured at 50x magnification over a height of 10 μm due to the increase in slope (See Fig. 5.13). The measured data was fit to a least squares arc based on the equation of a circle such that the radius of curvature (ROC) could be determined. The residuals of the fit then were averaged to determine the roughness of the given profile. Figure 5.13 shows that the spherical indenters are very close to their design specifications. The replicated lithium profiles, however, exhibit significant scatter with respect to both their figure and finish as shown in Table 5.2 below. Such scatter is likely due to the poor surface characteristics of the lithium foil as received. Freshly extruded ingot that has been cold rolled into foil is expected to perform far better than the commercially obtained lithium foil used here. Parabolic profiles have not been successfully replicated as of yet due to trapped air pockets at the tip of the profile during cooling. Vacuum impregnation of the replicating media while curing is the most viable solution to this problem and has yet to be tried.

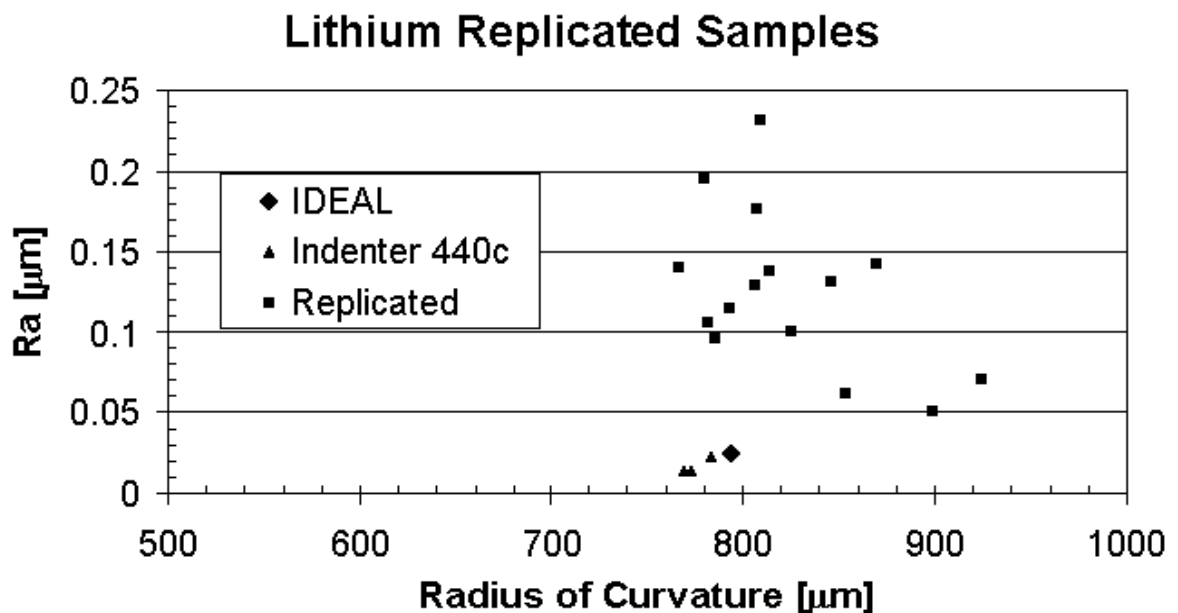


Figure 5.13. Radius of Curvature and Roughness Measurements via White Light Interferometer.

Table 5.2. Statistics of Replicated Sample Measurements.

	Mean	Standard Deviation
ROC [μm]	833.4	60
Ra [mm] ($\mu\text{in.}$)	0.16 (6.34)	0.148 (5.8)

5.5 Testing of a Lithium Compound Refractive Lens

Using the methods described in Sections 5.2 and 5.3, a lithium compound refractive lens was built for use on beamline 7ID at the Advanced Photon Source (APS). Beamline 7ID layout is shown below in Figure 5.14. The undulator generated a 270 μm *rms* beam in the horizontal and an 8.8 μm *rms* beam in the vertical. The L5 with a 0.5 x 0.5 mm aperture was placed 26.5 m from the source to limit the size of the source in the horizontal direction. A cryogenically cooled double crystal Si (111) monochrometer isolated the desired energy of the beam. A coherent slit is placed just before the lithium lens to allow only those portions of the beam that will enter the lens aperture to pass. The lithium lens itself (See Fig. 5.15) consisted of 32 parabolic lenslets with a 100 μm radius of curvature at the tip and a 0.6 mm aperture and were fabricated with the 316 stainless steel parabolic tips. (See Fig. 5.8) This lens design corresponds to a focal length of 1.7 m at an energy of 10 keV. The detector at the focal length consisted of a cerium-doped YAG crystal used as a scintillator and a 12-bit charge coupled (CCD) camera (Photometrics CoolSNAP HQ) equipped with a 2x lens objective. The CCD detector has a 1392 x 1040 pixel imaging array with 6.45 x 6.45 μm pixels. The 2X objective lens increases the camera resolution to 3.23 x 3.23 μm per pixel.

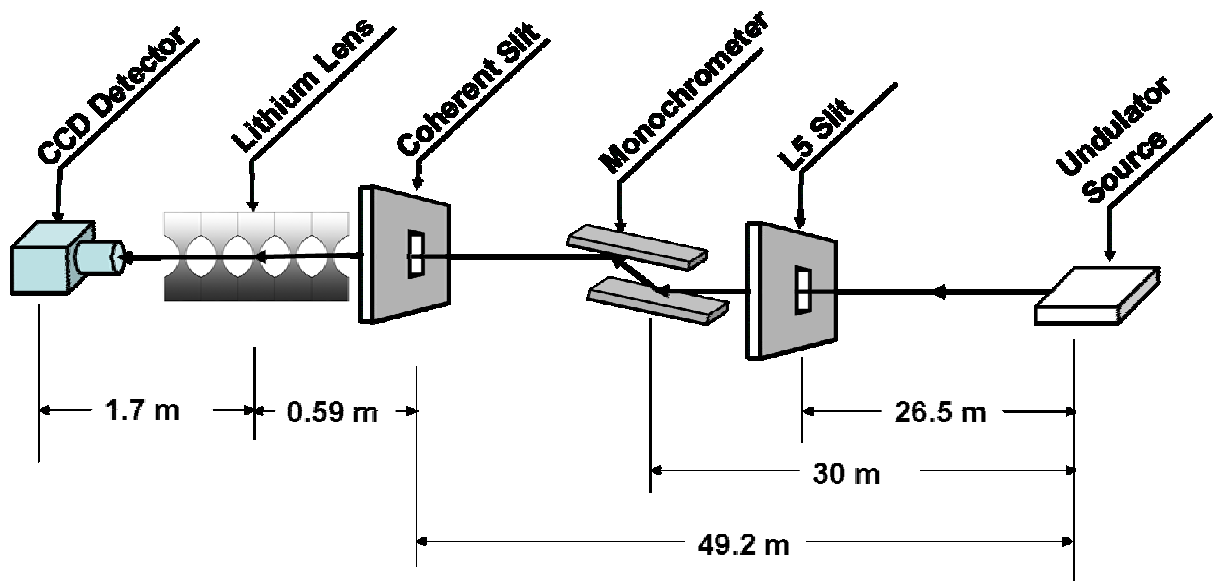


Figure 5.14. Schematic Layout of Beamline 7ID.

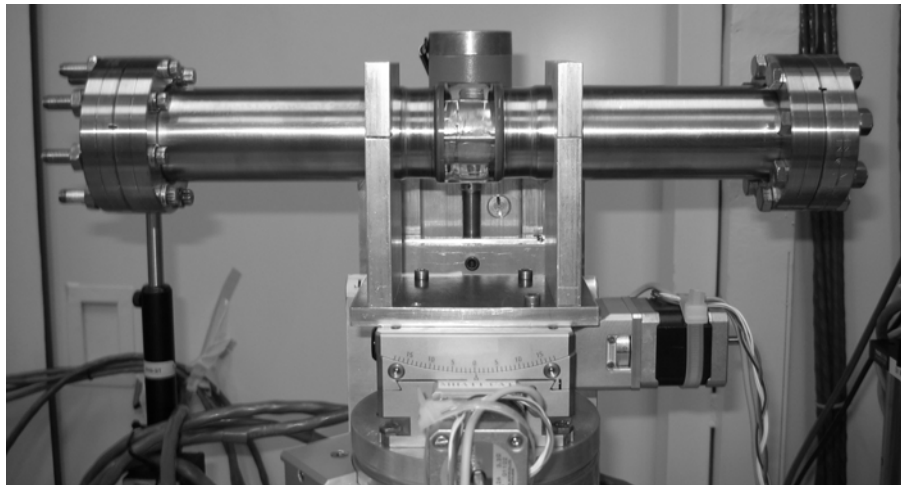


Figure 5.15. Picture of Lithium Compound Refractive Lens in the Beamline.

Testing of the lens consisted of measuring the location and size of the focal spot, the gain of the lens, and the transmission of the lens. Once the lens and detector were centered on the beam, the size of the focal spot was measured along the beam path to find the smallest focal spot. The smallest focal spot size was measured at a focal length of 1.71 m, just 10 mm from the theoretical focal length of 1.7 m as shown in Figure 5.16. The measured vertical and horizontal full-width at half-maximum (FWHM) of the focused beam was $23.7 \mu\text{m}$ and $34.3 \mu\text{m}$ respectively (See Fig. 5.17). Theoretical calculations expected a horizontal and vertical FWHM of $0.7 \mu\text{m}$ and $22 \mu\text{m}$ respectively. Figure 5.18 compares the size and structure of an

unfocused beam with that of a focused beam at the focal spot. The increase in peak intensity between the unfocused and focused beams (gain) was measured to be 18.4. Theoretical gain using Equation 4.2 yielded a value of 64 when considering the entire aperture of the lens (0.6 mm) to be the effective aperture.

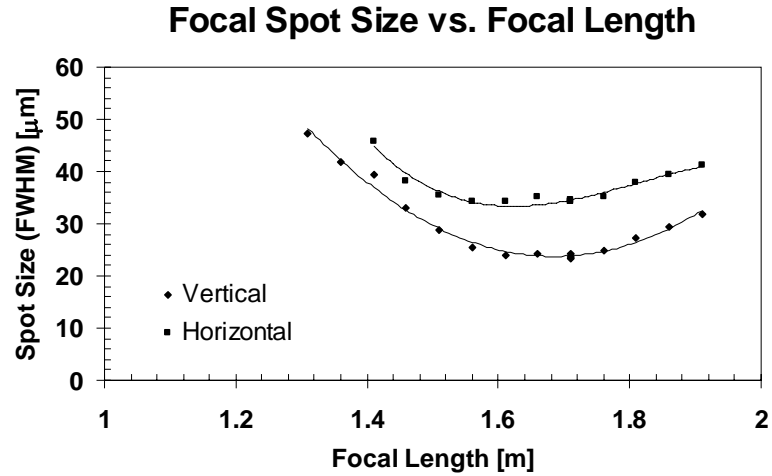


Figure 5.16. Plot of Focal Spot Size (FWHM) vs. Focal Length.

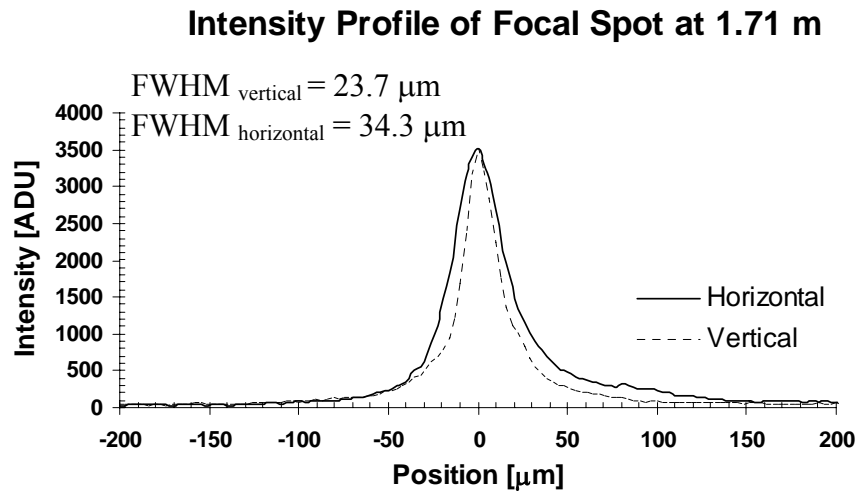


Figure 5.17. Intensity Profile of Smallest Focal Spot.

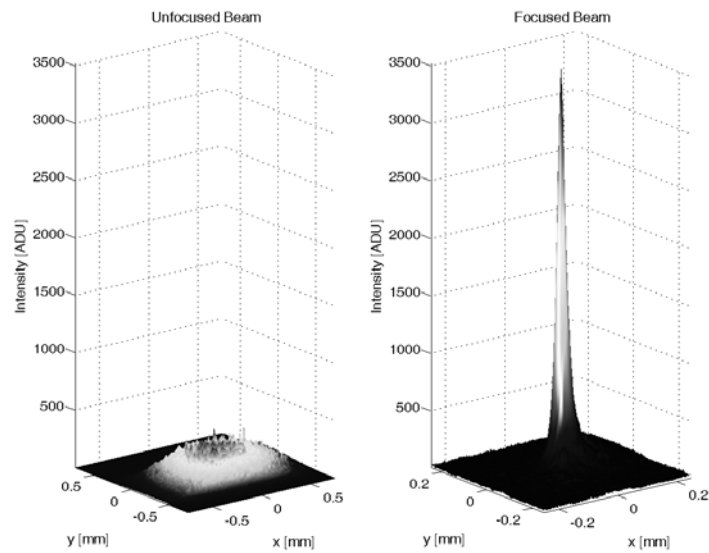


Figure 5.18. 3D Intensity Profiles of Focused and Unfocused Beam at the Focal Spot.

Once the smallest focal spot was identified, the transmission of the lens was investigated. Transmission refers to the number or percentage of x-rays that pass through the lens compared to the incident beam. Theoretically, transmission is calculated via Equation 4.1, however experimentally an ion chamber detector is placed right after the lens and counts the number of x-rays passing through the lens as a very thin beam scans through the aperture as shown below in Figure 5.19. Such scans can be used to approximate the cumulative thickness of the individual lenslets to identify possible figure or misalignment errors present in the lenslets. Figure 5.20 shows the result of solving Equation 4.1 for thickness and comparing the parabolic profile of the combined thickness of all of the lenses compared to theoretical calculations. Applying a second degree polynomial curve fit to the experimental lens profile yielded a radius of curvature of the lenses to be $109\ \mu\text{m}$ and can be compared with the design ideal of $100\ \mu\text{m}$.

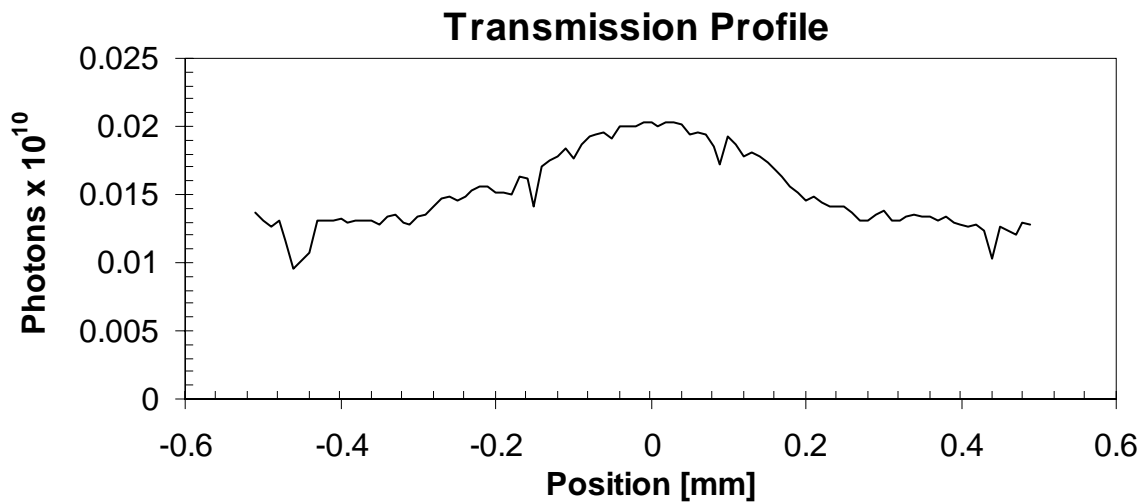


Figure 5.19. Transmission Profile of the Lithium Lens

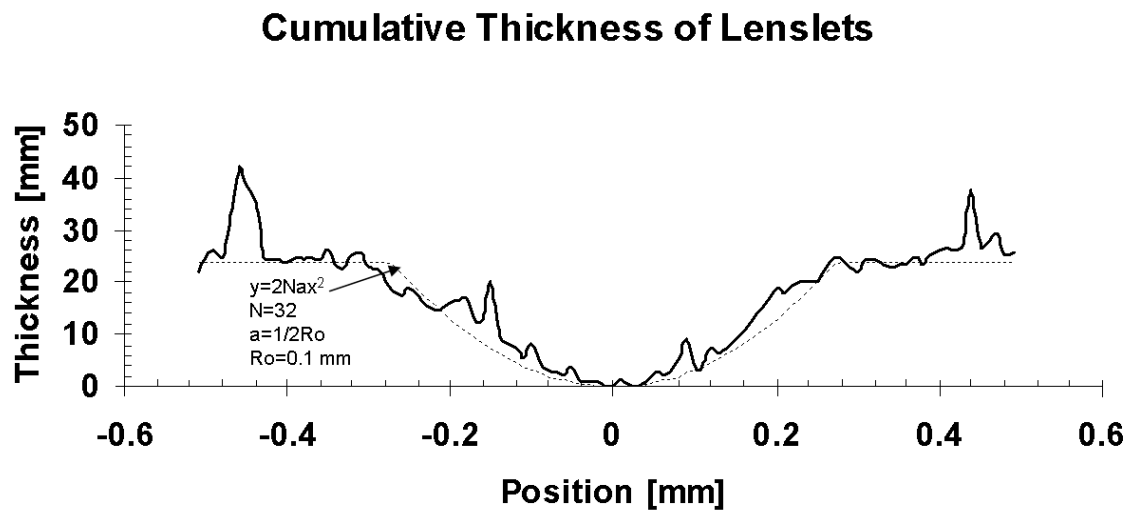


Figure 5.20. Theoretical vs. Experimental Cumulative Thickness of Lithium Lenslets.

Overall, the lithium compound refractive lens functioned well as an x-ray optic. Its performance with respect to gain and focal spot size are competitive with previously reported lithium lenses. Improvement in performance is easily attainable with 316 stainless steel indenters fabricated with higher precision lathes and commercial eletropolishers.

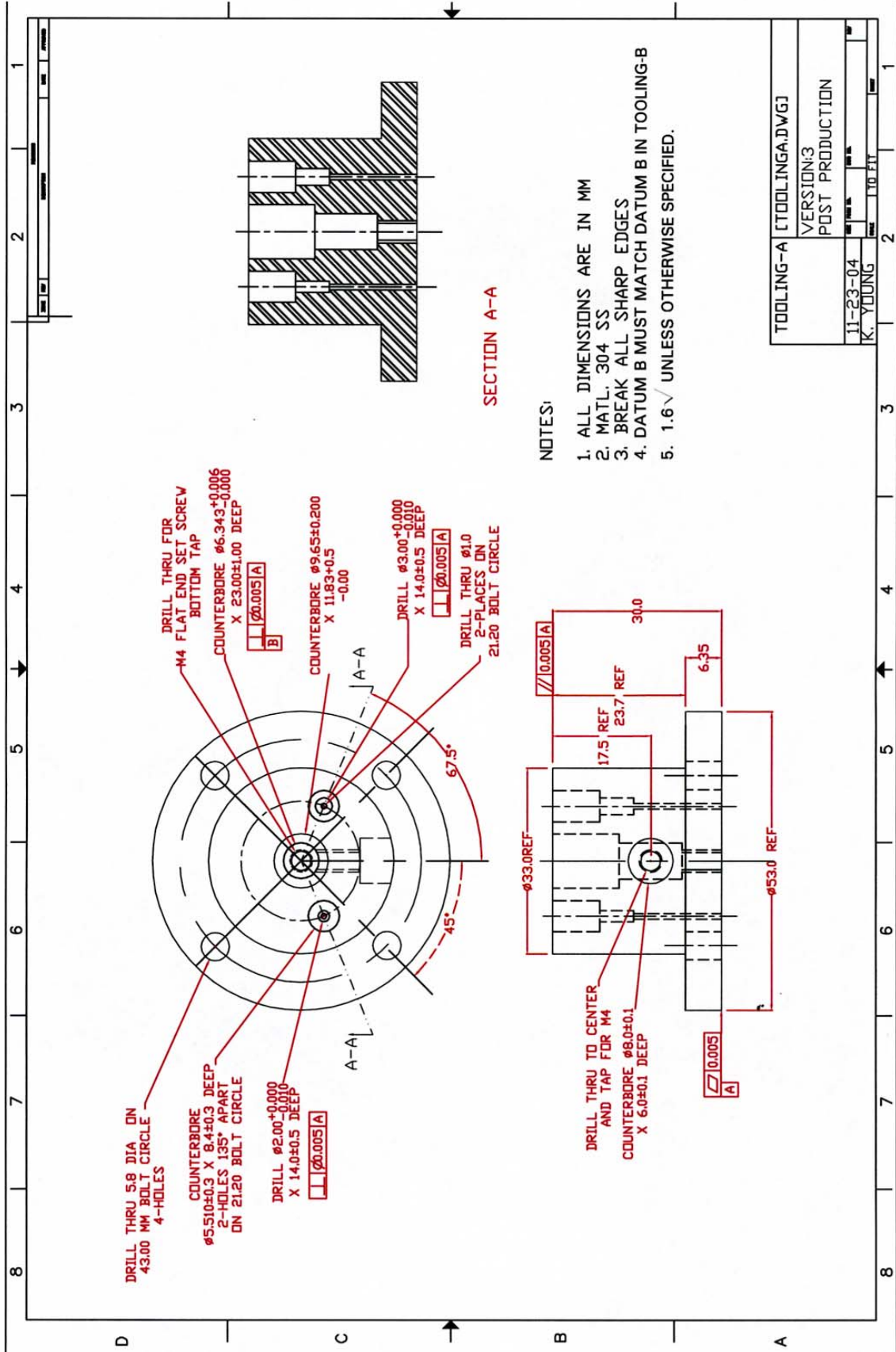
5.5 Future Work

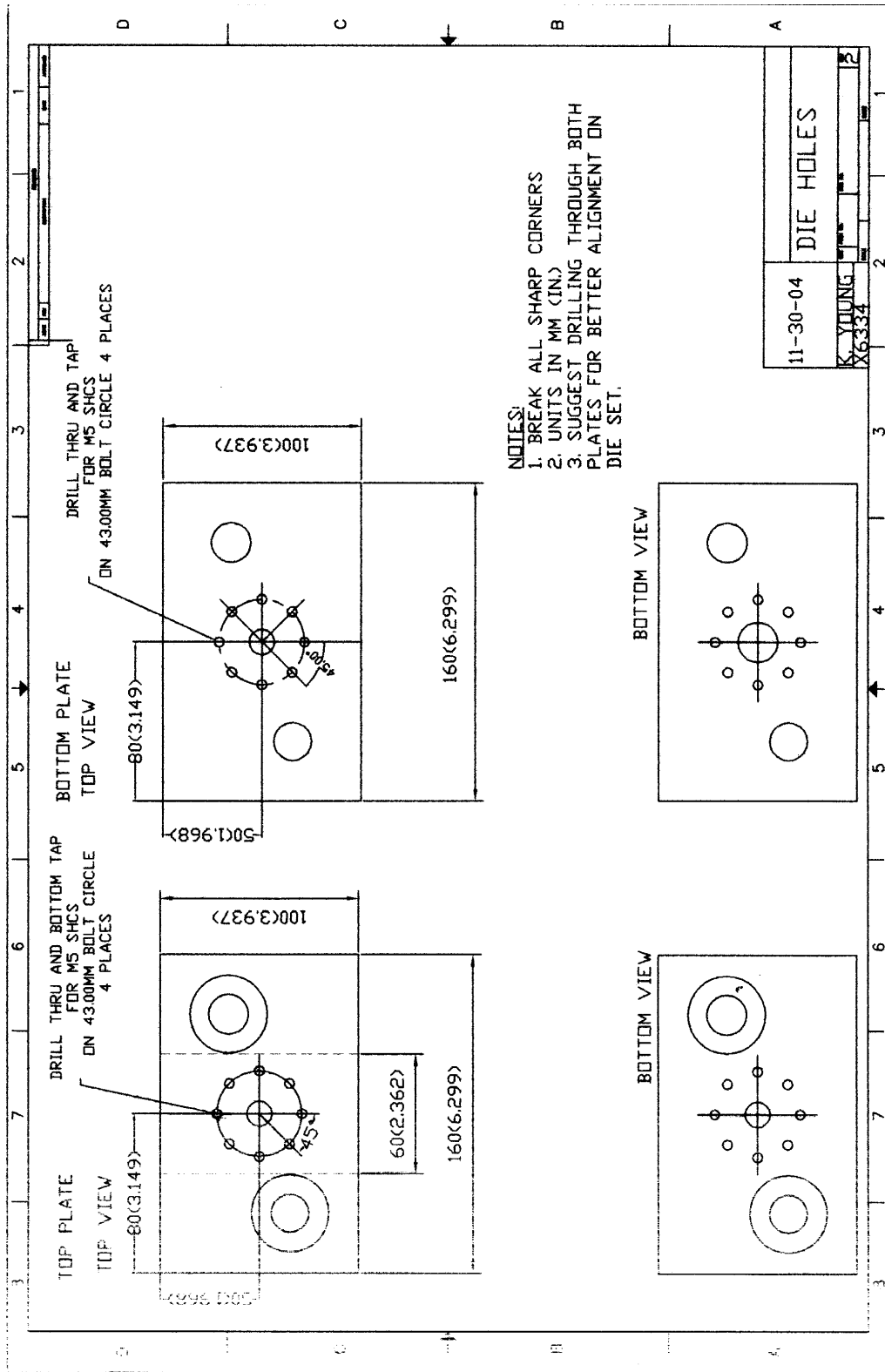
The work performed thus far lays the foundation for the assembly and testing of high performance lithium compound refractive x-ray lenses. The design utilizes novel tools that currently exist in industry to serve as spherical indenters to provide a near optical quality

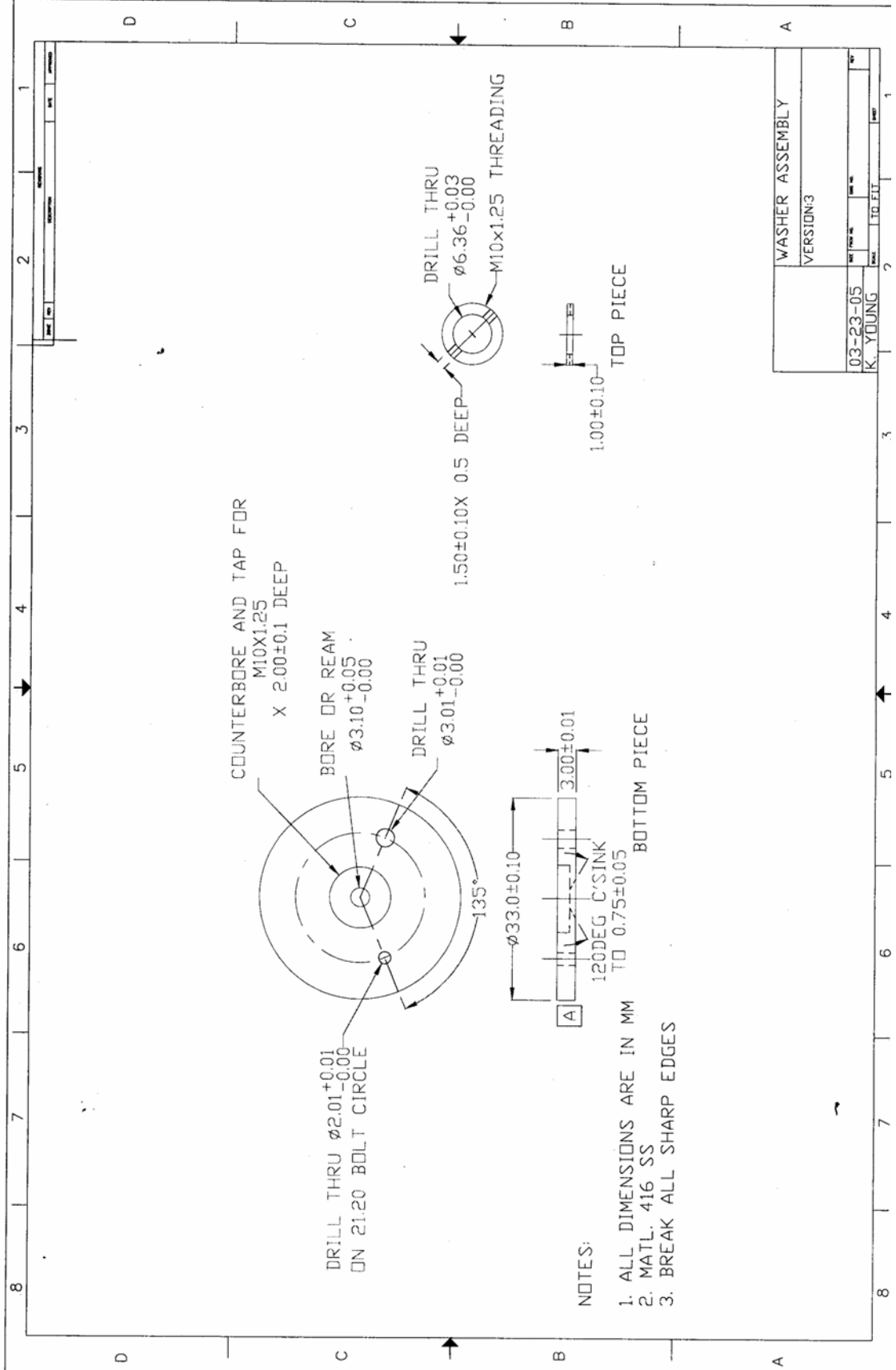
component to induce the deformation in the lithium foils. Also, this is the first instance that electropolishing has been used as a means to achieve an accurate parabolic profile with a good surface finish. In addition, measuring techniques to quantify the figure and finish of the lenslet profiles allows for a means of quality assurance such that the best settings of the press can be dialed in to achieve the best profiles. Lastly, given the tight tolerances of the press, and the cartridge units, the overall alignment of the unit is expected to be exceptional. All of the above considerations lead to the expectation that the CRLs produced at the APS will not suffer from the same figure and finish limitations as described in previous published work on lithium CRLs. The next steps would be to refine the lenslet characterization techniques and in turn the die press settings for the best finish with regard to both spherical and parabolic profiles to assemble a lithium CRL. Other indenter materials and manufacturing methods can also be explored. In addition, a better understanding of the mechanical behavior of lithium during the pressing process could lead to better design considerations to account for phenomena such as springback if they occur. Finite element modeling of lithium during the pressing process would be able yield important information in this regard.

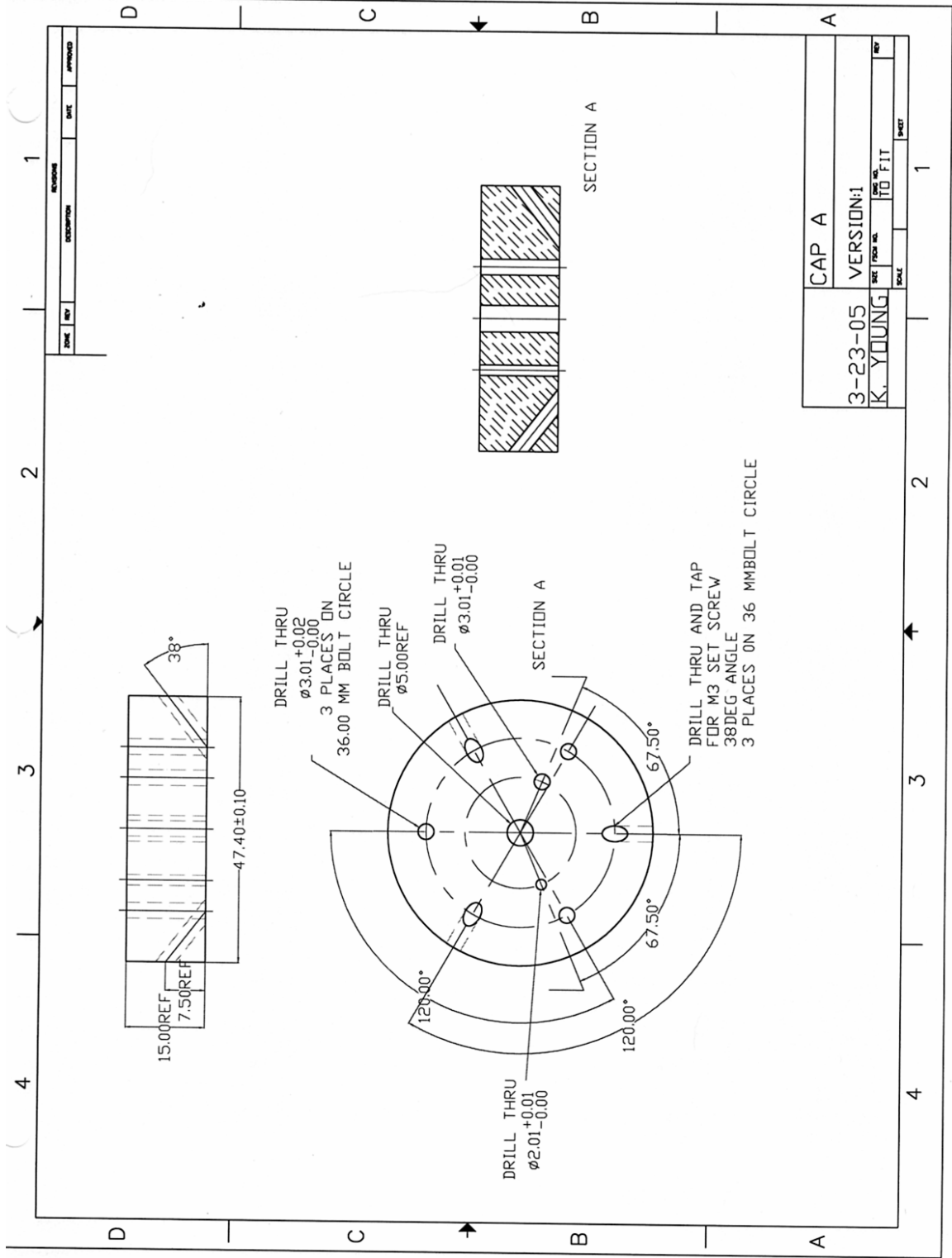
APPENDIX A

CAD DRAWINGS OF LITHIUM LENS DESIGNS



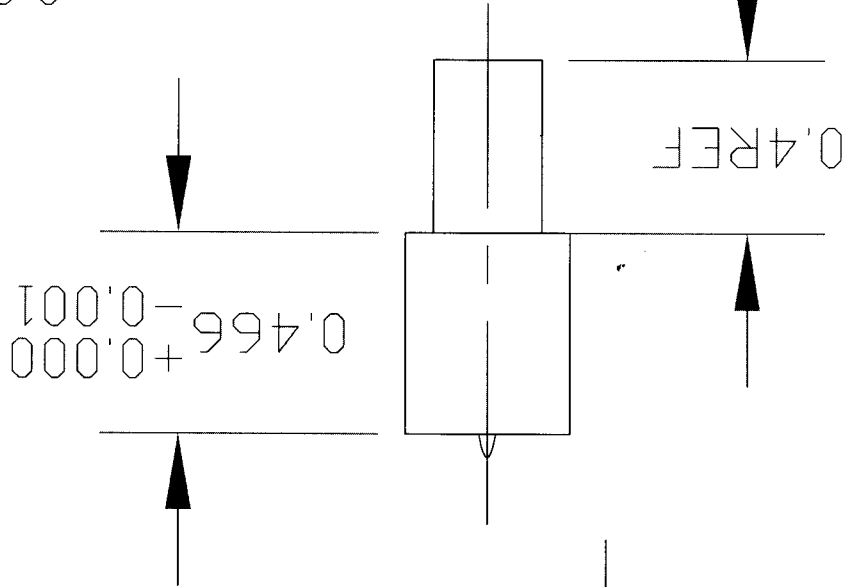
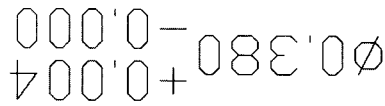
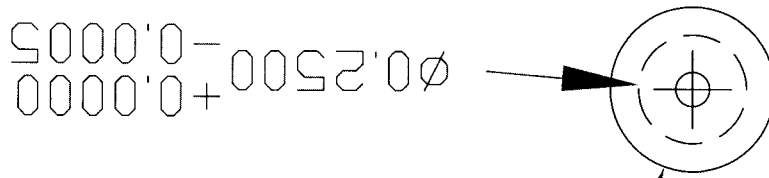






SHEET		SCALE		K. YOUNG	
REV		SIZE		2-16-05	
DWG NO.		FSCM NO.		VERSION: 1	
INITIAL DESIGN		parabolic indenfor.dwg			

NOTE:
 1. ALL DIMENSIONS IN ENGLISH
 2. MATL. 430.55
 3. ALL SURFACES 32 MICRO-INCH
 EXCEPT PARABOLIC TIP



REVISIONS			
ZONE	REV	DESCRIPTION	DATE

APPROVED

APPENDIX B

SAFE HANDLING OF LITHIUM

Purpose

Refractive lenses are used to focus x-ray beams. Lithium is particularly suitable as a refractive lens because of its relatively high index of refraction and its low absorption. Lithium lenses may be developed by extrusion, molding, pressing or stamping. This document lists the necessary safeguards and provides a procedure for handling lithium for this purpose. Each fabrication method will be performed on an experimental basis and the one that works best will be adapted.

Scope

This procedure describes safe handling and disposal of lithium during the fabrication of a refractive x-ray lens.

Principal Hazards

1. Lithium is an alkali metal.
2. Lithium is moderately corrosive and moderately flammable. In case of injury or uncontrollable fire, dial 911.
3. Lithium is highly reactive to water, and to moisture in air, and is highly reactive at temperatures above its melting point (180.5 °C).
4. Lithium reacts with body moisture to form corrosive lithium hydroxide, which can cause a chemical burn. Do not expose the skin, eyes, nose or throat to lithium. Prolonged exposure to lithium can cause:
 - a. Eye irritation, severe damage to the eyes or blindness.
 - b. Skin damage or irritation.
 - c. Irritation to the nose or throat.

5. Do not expose lithium to water, sources of water (e.g., sprinkler systems), or water vapor in moist air:
 - a. Lithium reacts violently with water in an exothermic reaction to form flammable hydrogen gas and lithium hydroxide.
 - b. The heat of this reaction may be enough to melt the lithium, leading to a secondary reaction where the released hydrogen gas is ignited, possibly resulting in an explosion that would scatter corrosive lithium hydroxide and form lithium oxide dust. Lithium oxide can cause a chemical burn to lung tissue if inhaled. **Note: The rate of reaction of lithium increases as the exposed Li surface area increases.**
6. Lithium is flammable and should not be exposed to spark-generating equipment or to an open flame in the presence of air. Burning lithium releases corrosive lithium oxide dust and fumes. Make sure any spark-generating equipment is grounded.
 - a. Fine particles, shavings, and foils of lithium ignite easily from sparks.
 - b. Blocks, ingots and rods (e.g., 1/2" diameter rods) do not burn easily when exposed to a spark.

Precautions

1. Use the appropriate personal protective equipment and take the appropriate precautions when handling lithium.
2. Refer to the Materials Safety Data Sheet for measures to be taken in case of accidental exposure (e.g., to eyes or skin).
3. Handle lithium in a conditioned glove box or dry room environment.
4. When physically handling lithium:
 - a. Latex gloves must be worn.
 - b. Tongs should be used.

- c. In the case of an accidental scattering of lithium, use the cleanup procedures described in Appendix C.
5. Have materials that can extinguish a small lithium fire, such as graphite or Lith-X, readily available in all locations where lithium is handled. **Note: Do not use water, sand, or carbon dioxide to extinguish a lithium fire.**
 - a. Lith-X is used to smother a lithium fire by removing the oxygen for the flame to burn.
 - b. Lith-X can be administered by shoveling it or scooping it onto the flame.
 - c. If a lithium rod is accidentally dropped into water and ignites, it must first be taken out of the water with tongs before dousing it with Lith-X. **Note: Lith-X powder will separate if placed in water.**
6. Provide electrical grounding for the table on which lithium work is carried out.

Limitations

1. A maximum of 250 grams of lithium may be used in each experimental setup.
2. The quantity of lithium in use must not exceed 250 grams and the amount stored must not exceed 480 grams.
3. Lithium should be handled in a glove box or dry room environment. Lithium in small quantities can be handled in air for short periods of time only if all recommended personal protective equipment is worn. However, the lithium will quickly corrode in air.
 - a. For work in an unsealed glove box, flowing argon gas can purge air making the environment suitable for working with lithium. Because of its higher atomic weight, argon causes stratification of the air in the glove box, causing the air to flow out the ventilation hole near the top of the glove box. Argon does not mix readily with air and will displace the air easily.

- b. The flow rate is kept very low (see MSDS) and it is not necessary to exhaust the argon gas into a laboratory exhaust system, however the necessary equipment is provided to do so if necessary.
4. A heater if needed may be employed to raise the temperature of a small quantity of lithium to no more than 150°C to increase its formability.
 - a. The heater used will be inspected to ensure that there are no sources of sparks.
 - b. The work must be performed in a glove box or under a fume hood if the lithium is to be heated to a temperature where fumes are generated.

Personal Protective Equipment

1. Latex gloves for handling lithium if working outside of a sealed glove box.
 - a. Latex gloves may also be worn before putting hands in the glove box for added protection against accidental exposure to skin due to any holes or punctures in the glove box gloves.
2. Safety glasses with side shields and a face shield if necessary should be worn when handling lithium outside of the glove box.
3. A laboratory coat and/or long sleeve clothing to protect the skin from exposure to lithium.
4. Safety glasses and face shield may be removed once the lithium is placed in the glove box.

Arrival, Packaging and Labeling of Lithium

1. If the stored lithium is not intended for immediate use, it should remain sealed in its shipping canister until ready for use. If the lithium has already been removed from its shipping canister, it should be stored under mineral oil, or in a dry room or glove box. The lithium container should be placed in a flammable storage cabinet.
2. Lithium is usually packaged in a hermetically sealed container that is filled with argon or mineral oil.

3. Packages with lithium must bear labels that say "Flammable Solid" and "Dangerous When Wet."
4. In spite of packaging, lithium should be used as soon as possible after it has been received.
5. Ensure that the lithium (quantity, location, responsible personnel) is entered into a chemical inventory database.

Work Process:

1. Put on the necessary personal protective equipment
2. Put material, equipment and a marked container of Lith-X in glove box or dryroom.
3. Go to a well-ventilated area and inspect the lithium container for signs of pressure build-up.
 - a. If a hissing sound is heard, if the lithium ignites, or if the container appears to be bulging, call 911.
4. Place the container of lithium in the glove box or dry room.
 - a. Open the container and carefully place the lithium on a spill tray.
5. If necessary, heat the lithium to a temperature no more than 150°C.
6. Store unused lithium in the designated storage area at the end of the day.
7. Follow the disposal methods outlined below for scrap lithium.

Establish a Receptacle for Waste Collection

1. Obtain an empty 250 mL waste disposal container filled with USP (heavy) mineral oil for scrap lithium. Containers should be high-density polyethylene or stainless steel.
2. Clearly mark the container with labels reading: "Lithium Scrap," "Flammable Solid" and "Dangerous When Wet."
3. Make sure that the container is either empty or has only the same waste material as the waste being generated. Do not mix waste materials.

4. Establish a new satellite accumulation area (SAA) for waste disposal. This should be in the same working area where the waste is produced and is under the control of the waste generator or the lab safety captain. This area must be used exclusively for lithium waste.

Cleanup and Storage of Lithium

1. Store any unused lithium in a safe area (i.e. flammable storage cabinet) isolated from any sources of water, acids, oxidizers, oxygen, nitrogen, and carbon dioxide.
 - a. Lithium should be stored in a container filled with mineral oil that is labeled with a description of the contents, quantity, investigator's name and lab telephone extension.
2. Storage areas should not be subject to high temperatures, sources of an open flame, or spark-generating equipment.
3. Flammable storage cabinets containing lithium should be clearly posted with labels designating the quantity of lithium, "Flammable Solid" and "Dangerous When Wet".

Disposal of Scrap Lithium

1. Any lithium waste should be placed in a sealed, container filled with mineral oil.
2. The waste constituents should be marked on the waste container.
3. Only small quantities of lithium should be disposed of at one time. Do not allow too much lithium scrap to accumulate. Consider disposing of lithium waste as soon as possible.

Spill Cleanup Procedure for Lithium

Below is a procedure to be used in the cleanup of spills that occur when handling lithium. If you do not feel confident in attempting to clean a spill, call the lab safety captain or dial 911 (based on the seriousness of the spill). **WARNING: Personnel must wear the appropriate personal protective equipment in order to perform a spill cleanup.**

Spill Cleanup Procedure

1. If there is no fire:
 - a. Cover spilled lithium with USP grade mineral oil.

- b. Place lithium in a disposal container (e.g., a polyethylene bottle), close the container securely and label the container with the contents, quantity, investigator's name, and lab telephone extension.
 - c. Wipe away any remaining traces of mineral oil.
 - d. Document spill cleanup activities, identify cause and determine actions that could prevent future spills.
 - e. Report the incident to the lab safety captain immediately.
2. If there is a small fire:
 - a. Extinguish the fire with either graphite or Lith-X.
 - b. Notify the lab safety captain immediately.
 3. If there is a large fire:
 - a. Dial 911.
 - b. Notify the lab safety captain immediately.

BIBLIOGRAPHY

- [Born99] Born, M., E. Wolf, and A. B. Bhatia. Principles of Optics: Electromagnetic Theory of Propagation, Interface, and Diffraction of Light. Cambridge, Eng.: Cambridge University Press, 1999.
- [Bro66] Brown, J. G. X-Rays and Their Applications. New York: Plenum Press, 1966.
- [Carp05] Young, Kristina. "Re:microXAM Q's." Email to David Macaulay. 1 April, 2005.
- [Ced02] Cederstrom, B., Lundqvist, M., and Ribbing. C. "Multi-prism X-ray Lens." American Institute of Physics 81 (2002): 1-3.
- [Chi04] Chi, T., T. Ballinger, R. Olds, and M. Zecchino. "Surface Texture Analysis Using Dektak Stylus Profilers." Veeco Instruments Application Notes. 15 May 2005 <http://www.veeco.com/appnotes/AN525%20_Dektak_Surface.pdf>.
- [Church95] Church, E. L., and P. Z. Takacs. "Specification of Glancing- and Normal-Incidence X-Ray Mirrors." Optical Engineering 34.2 (1995): 353-360.
- [Compt23] Compton, A. H. "The Total Reflection of X-Rays." Philosophical Magazine 45 (1923): 1121.
- [Compt54] Compton, A. H., and Allison, S. K. X-Rays in Theory and Experiment. New York: D. Van Nostrand Company, Inc., 1954.
- [Crem00] Cremer, J. T., M. A. Piestrup, H. R. Beguiristain, C. K. Gary, and R. H. Pantell. "Large Aperture Compound Lenses Made of Lithium." Review of Scientific Instruments 74.4 (2003): 2262-2266.
- [Duf01] Dufresne, E. M., D. A. Arms, R. Clark, N. R. Pereira, S. B. Dierker, and D. Foster. "Lithium Metal for X-ray Refractive Optics." Applied Physics Letters 79.25 (2001): 4085-4087.
- [Fzp05] NTT Advanced Technology Corporation. Fresnel Zone Plate. 2005. NTT Advanced Technology Corporation, San Bruno. 3 April 2005 <http://www.keytech.ntt-at.co.jp/nano/prd_e0002.html>.
- [Guz01] Guzowski, M., F. F. Kraft, and H. R. McCarbery. Micro-Multiport (MMP) Tubing with Improved Metallurgical Strength and Method for Making Said Tubing. Brazeway Inc., assignee. Patent 6,192,978 B1 Oct. 2001.
- [Hec90] Hecht, Eugene. Optics. Reading: Addison Wesley, 1990.
- [Hen82] Henke, B. L., P. Lee, T. J. Tanaka, R. L. Shimabukuro, and B. K. Fujikawa. "Low-Energy X-Ray Interaction Coefficients: Photoabsorption, Scattering, and Reflection: E=100-2,000 eV, Z=1-94." Atomic Data and Nuclear Data Tables 27.1 (1982): 1-144.

- [Hen93] Henke, B. L., E. M. Gullikson, and J. C. Davis. "X-Ray Interactions: Photoabsorption, Scattering, Transmission, and Reflection at $E=50\text{-}30,000$ eV, $Z=1\text{-}92$." Atomic Data and Nuclear Data Tables 54.2 (1993): 181-342.
- [How75] Howell, J. A., and Horowitz, P. "Ellipsoidal and Bent Cylindrical Condensing Mirrors for Synchrotron Radiation." Nuclear Instrumentation and Methods, 125 (1975): 225-230.
- [Ice00] Ice, G. E., Chung, J. S., Tischler, J., Lunt, A., and Assoufid, L. "Elliptical X-Ray Microprobe Mirrors by Differential Deposition." Review of Scientific Instruments 71 (2000): 2635.
- [Jep78] Jeppson, D. W., J. L. Baliff, W. W. Yuan, and B.E. Chou. "Lithium Literature Review: Lithium's Properties and Interactions." HEDL-TME 78-15. Hanford Engineering Development Laboratory. 1978.
- [Khou02a] Khounsary, A. K., Shastri, S. D., and Macrander, A. "A Variable-Focus Compound Lens." 2nd International Workshop on Mechanical Engineering Design of Synchrotron Radiation Equipment and Instrumentation (MEDSI02), pp. 58-64, 2002.
- [Khou02b] Khounsary A., S. D, Shastri, A. Mashayekhi, A. Macrander, R. Smither, F. F. Kraft. "Fabrication, Testing, and Performance of a Variable-focus X-ray Compound Lens." Proceedings of SPIE: Vol. 4873. Design and Microfabrication of Novel X-Ray Optics. Ed. Derrick Mancini. Bellingham: SPIE, 2002. 49-54.
- [Kirk48] Kirkpatrick, P., and Baez, A. V. "Formation of Optical Images by X-Rays." Journal of Optical Society of America 38 (1948): 766-774.
- [Kraft04] Kraft, F. "Re: Extrusion Question." E-mail to Kristina Young. 28 July 2004.
- [Laue81] Laue, K., and Stenger, H. Extrusion. Metals Park: American Society for Metals (ASM), 1981.
- [Leng99] Lengeler, B., Schroer, C. G., Richwin, M., Tümmeler, J., Drakopoulos, M., Snigirev, A., and Snigireva, I. "A Microscope for Hard X-Rays Based on Parabolic Compound Refractive Lenses." Applied Physics Letters 74 (1999):3924-3926.
- [Manc02] Mancini, D. C., Moldovan, N., Divan, R., DeCarlo, F., and Yaeger J. "X-ray Lenses Fabricated by Deep X-ray Lithography." Proceedings of SPIE: Vol. 4873. Design and Microfabrication of Novel X-Ray Optics. Ed. Derrick Mancini. Bellingham: SPIE, 2002. 28-36.
- [Mat05] Matweb.com. 2005. Material Property Data. 1 April 2005 <http://www.matweb.com/>.
- [Math99] Mathiesen, R. H., Arnberg, L., Mo, F., Weitkamp, T., and Snigirev, A., "Time-Resolved X-ray Imaging of Dendritic Growth in Binary Alloys." Physical Review Letters 83 (1999): 5062-5065.
- [Mich96] Michette, A.G., and S. Pfauntsch. X-Rays: The First Hundred Years. West Sussex, Eng.: John Wiley and Sons Ltd, 1996.

- [Pan01] Pantell, R. H., J. Feinstein, H. R. Beguiristain, M. A. Piestrup, C. K. Gary, and J. T. Cremer. "The Effect of Unit Lens Alignment and Surface Roughness on X-ray Compound Lens Performance." Review of Scientific Instruments 72.1 (2001): 48-52.
- [Per04] Pereira, N. R., E. M. Dufresne, R. Clarke, and D. A. Arms. "Parabolic Lithium Refractive Optics for X-rays." Review of Scientific Instruments 75.1 (2004): 37-41.
- [Pie00] Piestrup, M. A., Cremer, J.T., H.R. Beguiristain, C.K. Gary, and R. H. Pantell. "Two-dimensional X-Ray Focusing from Compound Lenses Made of Plastic." Review of Scientific Instruments 71.12 (2000): 4375-4379.
- [Rio98] Sánchez del Río, M., and R. J. Dejus. "XOP: Recent Developments." Proceedings of SPIE: Vol. 3448. Crystals and Multilayer Optics. Ed. A.T. Macrander, A. K. Freund, T. Ishikawa, and D. M. Mills. Bellingham: SPIE, 1998. 340-345.
- [Schr02] Schroer, C. G., Benner, B., Günzler, T. F., Kuhlmann, M., Zimprich, C., Lengeler, B., Rau, C., Weitkamp, T., Snigirev, A., Snigireva, I., and Appenzellar, J. "High Resolution Imaging and Lithography with Hard X-rays Using Parabolic Compound Refractive Lenses." Review of Scientific Instruments 73 (2002): 1640-1642.
- [Sim99] Simonovici, A., Chukalina, M., Drakopoloulos, M., Snigireva, I., Snigirev, A., Schroer, C., Lengeler, B., Janssens, K., and Adams, F. "X-ray Fluorescence Microtomography: Experiment and Reconstruction." Proceedings of SPIE: Vol. 3772. Developments in X-ray Tomography I. Ed. U. Bonse. Bellingham: SPIE, 1999. 328-337.
- [Snig96] Snigirev, A., Kohn, V., Snigireva, I., and Lengeler, B. "A Compound Refractive Lens for Focusing High-Energy X-Rays." Nature 384 (1996): 49.
- [Snig98] Snigirev, A., Kohn, V., Snigireva, I., and Lengeler, B. "Focusing high-energy X-rays by Compound Refractive Lenses." Applied Optics 37 (1998) 653-662.
- [Tar03] Tariq, S. K. Ammigan, P. Hurh, R. Schultz, P. Liu, and J. Shang. "Li Material Testing: Fermilab Antiproton Source Collection Lens." Proceedings of the 2003 Particle Accelerator Conference, May 12-16, 2003. Ed. J. Chew, Peter Lucas, and Sara Webber. Piscataway: IEEE, 2003. 1452-1454.
- [Tin02] Tinsley Laboratories. Nanofocus Mirror Fabrication and Test Feasibility Study Report. Richmond: Tinsley Laboratories, 2002.
- [Van02] Vander Voort, G.F. Metallography: Principles and Practice. Materials Park: ASM International, 1999.
- [Win94] Winick, H. Synchrotron Radiation Sources: A Primer. Singapore: World Scientific, 1994.
- [Yam03] Yamauchi, K., Yamamura, K., Mimura, H., Sano, Y., Saito, A., Endo, K., Souvorov, A., Yabashi, M., Tamasaku, K., Ishikawa, T., and Mori Y. "Two-Dimensional Submicron Focusing of Hard X-Rays by Two Elliptical Mirrors Fabricated by Plasma Chemical Vaporization Machining and Elastic Emission Machining." Japanese Journal of Applied Physics 42 (2003): 7129-7134.

[Yang93] Yang, B. X. “Fresnel and Refractive Lenses for X-rays.” Nuclear Instruments and Methods in Physics Research A328 (1993): 578-587.

[Zec05] Zecchino, Mike. “Characterizing MEMS Devices through Transparent Media.” Veeco Instruments Application Notes. 15 May 2005
<http://www.veeco.com/appnotes/AN528_Characterizing_MEMS.pdf>.